Visualising Conformational Changes in HSP90 Protein using Plasmonic Nanoapertures

Christian Primavera

4586786

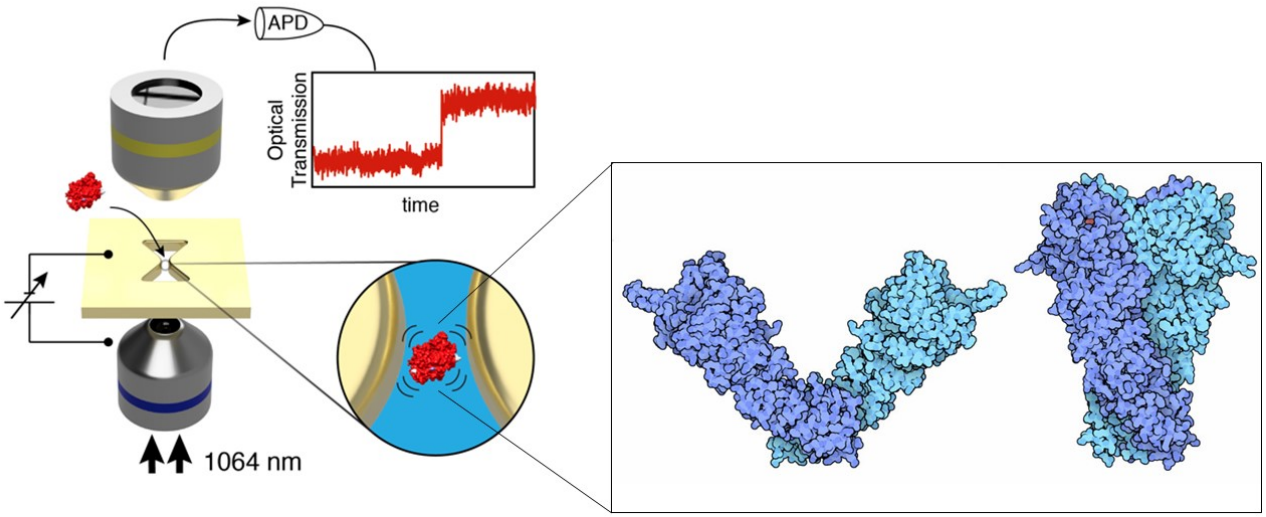

TU Delft Bachelor End Project, January 2020
BSc Applied Physics / BSc Applied Mathematics
Assessed by C. Dekker, J.L.A. Dubbeldam, C. Joo and F.J. Vermolen
To be defended on Tuesday February 18, 2020 at 9:00 a.m.
This thesis is available at https://repository.tudelft.nl/

-

Abstract

In this thesis, we demonstrate optical trapping of HSP90 proteins in plasmonic nanoapertures to study the HSP90 conformational change. This technique is label-free and non-destructive. The resonance of the bow tie shaped plasmonic nanoaperture is used to create a very strong electric field gradient force able to trap proteins. The resonance phenomenon is also used for detecting the trapping events, using the change in transmission that results from the presence of a protein in the trap. HSP90 can be trapped very stably for upwards of 30 seconds. The signal resulting from trapping HSP90 significantly differs from signals from bead traps, especially in the low-frequency regime. We observe strong evidence for a two level system when HSP90 was incubated with AMP-PNP which should slow down the conformational change (fit with $R^2 = 0.9988$). More work is required to demonstrate whether this two level system results from the conformational change. We conclude that there is a need for more advanced statistical methods to more conclusively prove that the HSP90 undergoes conformational change between two main levels and suggest further improvements to the experiments.

-

Acknowledgements

This thesis would never have come into existence if it had not been for the effort of some others that helped me throughout this process.

I would like to thank Wayne Yang, my direct supervisor, for guiding me through the entire process. I want to thank him for all the time and effort he put into this project, from getting me up to speed with running the experiments to giving numerous tips on the writing of this thesis.

I would like to thank Madeleine van Dijk for assisting me during all of the lab work that was required for obtaining the data. Her experience with the setup and in dealing with experimental issues were a great help for obtaining the data.

Further, I would like to thank professor Cees Dekker and professor Johan Dubbeldam for helping me set up this project as a combination of physics and mathematics. I would like to thank them for all the discussions about the subject throughout the project.

Lastly, I want to thank Chirlmin Joo and Fred Vermolen for assessing this thesis and for conducting the defence interview.

-

Contents

-

1 Introduction

Heat Shock Protein 90 (HSP90) is one of the most abundant proteins in all living cells. HSP90 functions as a chaperone protein, meaning it assists other proteins during their folding process and can keep them from denaturing if necessary. HSP90 can do this to many other proteins, so its function is ultimately important to all kinds of cellular processes, among which the stabilisation of some growth factor receptors. This one function makes HSP90 an interesting subject to study for the field of oncology, since many tumor-related proteins are assisted in their folding by HSP90 [12]. To perform its function, HSP90 undergoes a conformational change. Knowing more about the characteristics of this confomational change can be beneficial to the development of techniques that influence the function of HSP90.

The conformational change has already been studied before with more conventional methods. One example of this is using fluorescence resonance energy transfer (FRET), which relies on labelling two parts of the protein in order to determine the distance between the two labelled parts of the molecule. In figure 1, the results of determining the conformational change rates using FRET have been shown. We see that the largest changes (from open to closed) take place in a frequency regime slighly under 1Hz. We will come back to this in the theoretical background. Another technique that can be used is cryo electron microscopy (CryoEM). This involves plunge freezing the sample using liquid ethane, followed by an inspection in an electron microscope. All of these methods have in common that they rely either on labelling or on inspecting the proteins at a single moment in time. Most importantly, the dynamics of the protein have to be inferred indirectly. This is especially true in the case of CryoEM, where the different states are 'frozen' in time during the plunge freezing process. Both methods are shown in figure 1.

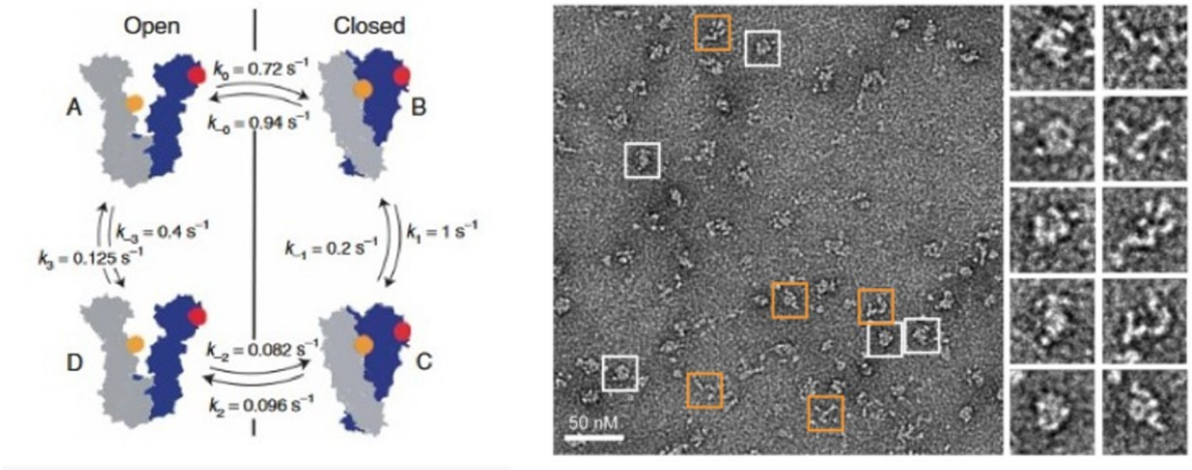

Figure 1: Conventional methods of studying conformational change in HSP90 protein. On the left, we see a schematic overview of the FRET technique used in [9]. We see that the two labels have been attached to the two monomers. From their relative distance, it is determined in which state the protein resides. On the right, we see a Cryo-EM picture from [17]. The sample has been plunge frozen and the conformations of the proteins are made visible using electron microscopy. The fraction of proteins in one state gives some information about the conformational change.

Optical trapping assisted by plasmonic nanoapertures knows none of these disadvantages. Using this technique, we can trap a single protein and observe it for seconds on end, allowing it to undergo several cycles of conformational change to build statistics. Also, we can observe it using properties of the trap, making this technique label-free. These large advantages make this technique very promising, since it is almost completely non-invasive. In the future, it might even be used in vivo, because it does not require any added chemicals or extreme temperatures.

The conventional way of optical trapping has existed since 1970. It was originally developed by Arthur Ashkin, who showed that dielectric particles from $10\mu m$ down to $25nm$ can be trapped using a focused laser beam [1]. The explanation for micron sized particles uses ray optics, shown in figure 2. It is based on the fact that the light rays carry momentum, and that it takes force to alter their direction, which happens because of the refractive index of the particle. Newton's third law tells us that the particle should be affected by a force equal in magnitude and opposite in direction. All the rays together then cause the particle to be forced back to the centre. For smaller particles, the explanation is based on a balance between the optical gradient force and the optical scattering force, which we will be dicussed in chapter 2 of this thesis. Ashkin received a Nobel Prize for the development of this technique that is now widely used.

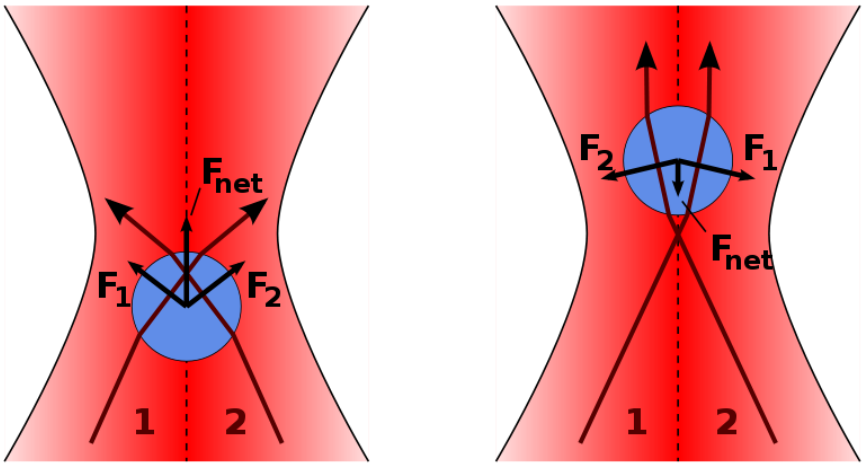

Figure 2: Optical trap explained with ray optics [8]. The explanation is based on Newton's third law. The incident light rays carry a momentum with them, with $p = E/c$. The refractive index of the particle causes the ray to change direction, for which a force is required. By Newton's third law, the ray must exert a force on the bead in the opposite direction. These forces are drawn in the figure, as well as the resulting force, from which we conclude that the particle will always be forced towards the point where the laser intensity is highest.

Since this discovery, the use of optical trapping has been extended to sub wavelength regimes through the use of plasmonics and nanostructures that are able to further focus the light into sub diffraction volumes. Nanoaperture assistance of this phenomenon has some additional advantages. Firstly, we are able to create a much steeper gradient in the electric field, which is amplified by the resonance of the aperture. This enables us to trap even smaller particles, like single proteins. Proteins as small as beta-amylase, dCas9 (90kDa) have already been trapped [19]. Secondly, we need a lower laser power to achieve trapping, since the electric field is amplified. This has several advantages for reducing heat damage as we will demonstrate in Chapter 2. Thirdly, there is no need for additional labelling of the protein, because the trapped particle affects the transmission, allowing for direct detection.

Objectives and goals of this thesis

Our goal is to show conformational changes in HSP90 protein by use of optical trapping in plasmonic nanoapertures. In this thesis, we will begin by introducing the technique. A simple model of the system will be built to understand how heat is dissipated in the nanoplasmonics aperture and key advantages compared to conventional optical trapping will be shown. After that, we will turn to experiments and show how the nanoapertures are fabricated, we will explain the setup and we will introduce the concepts for the signal analysis. We will continue by trapping HSP90 and comparing its signal to the signal of trapped polystyrene beads. These results will be analysed and we will investigate the influence of AMP-PNP on the conformational change in HSP90. While presenting the results of the experiments, we will investigate their implications and the remaining uncertainties, followed by suggestions for further research that can be done to extend our knowledge of this subject. The thesis will be concluded by summarizing the results we have encountered throughout the process.

2 Theoretical Background

The background information behind conformational changes in HSP90 protein will be discussed here, as well as the reasons why optical trapping in nanoapertures is a good method to study this change. We will also create some models of the situation to show what happens during a trapping event.

2.1 Conformational Change in HSP90

HSP90 is a protein abundantly found in almost all living cells [2]. It is classified as chaperone protein, meaning it assists the folding process of other proteins, and as ATPase protein, meaning it hydrolyses ATP into ADP during its function. Its name comes from the fact that it is expressed more in cells that are stressed by heat [3], where it functions by keeping other proteins from denaturing and hydrolysing dysfunctional proteins. It receives the '90' from the fact that each monomer has a size of roughly 90 kDa, which means the total size of the protein is approximately 180 kDa.

It is known from literature that HSP90 undergoes a conformational change during its operation as a chaperone protein, which has previously been proven using the FRET technique [9]. The conformational change that HSP90 undergoes, is shown in figure 3. The conformational change results in a large displacement of the monomers (the two parts of which the entire complex consists).

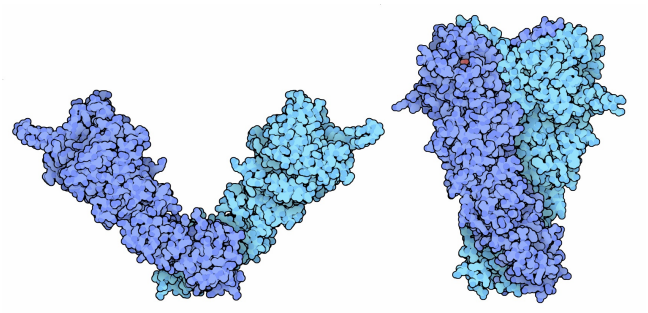

Figure 3: The two conformational states of HSP90, figure used from [16].

We expect the most significant changes, between the opened and closed states, to take place with a rate that is slightly less than once per second [9], as can be seen in figure 4.

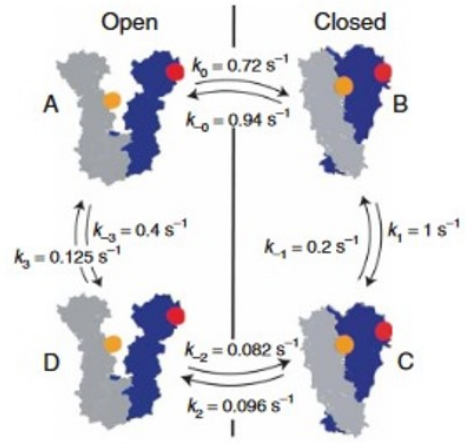

Figure 4: Conformational change rates in HSP90 protein [9]. We see that the most significant changes (A-B and C-D) will show up in the spectrum just below 1Hz.

Knowing more about processes that affect this conformational change is beneficial to varying fields of study. Since HSP90 is involved in so many different processes, this can have impact on many varying fields that deal with cellular processes, from pharmacology to industrial processes for synthesising chemicals using bacteria.

2.2 Nanoaperture Assistance of Optical Trapping

Optical trapping is a way of keeping a particle in one place by using light, without having to physically attach it to another object. This phenomenon already arises on micron scale. A good way of describing the situation is to calculate the electric field, which gives rise to the electric field gradient force. This is usually done using a FDTD (finite difference time domain) simulation. This way, we can still calculate the force the laser exerts on the trapped particle, while not relying on ray optics. The expression for the force becomes as follows in equation 1.

$$\vec{F}_{grad} = \frac{1}{2}\alpha V \vec{\nabla} E^2 \tag{1}$$

Equation 1 tells us that the particle will be drawn towards regions of a stronger electric field. The magnitude of the force is proportional to the square of the magnitude of the electric field and it is independent of the electric field direction. It also tells us that it is proportional to the volume of the particle.

The magnitude of the electric field can be enhanced by using a nanoaperture with a resonance wavelength close to the laser wavelength. These resonating structures could be shaped in numerous ways. Previously, all kinds of shapes have been tried [20], but the shape that is best at transporting the laser heat away from the trapping area, turns out to be an 'inverted bow tie', meaning we have a bow tie shaped hole in a conducting plate. The large gold area then serves as a heat sink.

This shape is good at conducting heat, but also still shows the resonance phenomenon. Figure 5 indicates how this works. If the laser is polarised in the same direction as the short end of the bow tie, the electric field is increased by a factor of almost 20 in the centre of the trap. If we rotate the polarisation by 90^o, the bow tie barely allows any electromagnetic waves to pass through.

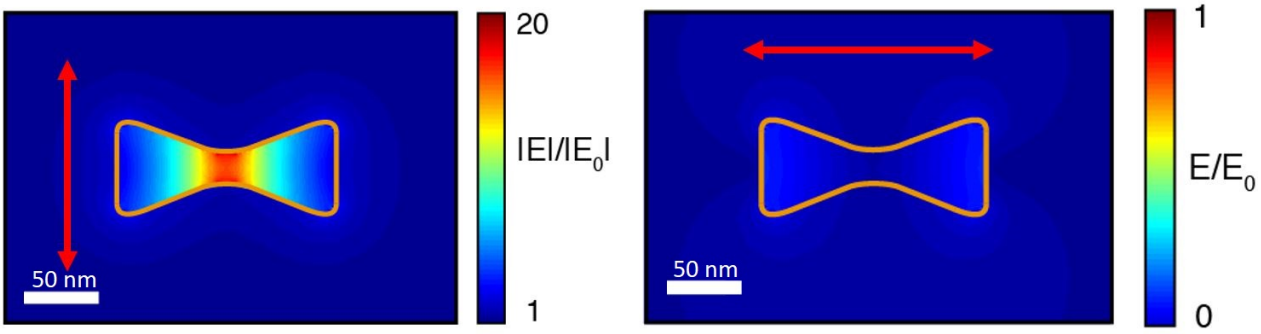

Figure 5: The result of a finite difference time domain simulation of the bow tie shaped antennae, under two polarisation directions of a laser with 1064 nm wavelength. The left image shows the transmission when the laser polarisation direction is parallel with the antenna, the right image shows the transmission when the polarisation direction is orthogonal to the antenna. Pay attention to the color scales on the right. The result is clear: with the first polarisation, the electric field norm is amplified up to 20 times, while with the perpendicular case, the laser is almost completely blocked.

This enables us to obtain a larger trapping force with the same laser power, or conversely, we can use a lower laser power to create a trap of the required strength. Using a lower laser power is advantageous since it causes less heating, so less disturbance in the system, while still creating a stable trap. The most important consequence of this is a significant decrease in the heat generation in the area. In this way, we can make sure the studied proteins do not denature or change in any other way because of the measurement. We will explicitly demonstrate this advantage in section 2.4 where we look at the temperature distribution as a result of the incident laser beam.

The result of this phenomenon is that nanoaperture assisted optical trapping is a very good way of stably confining a single protein, with minimal impact on the protein to be studied. This makes it very well suited for studying the HSP90 conformational change of interest. In the part that follows, we will discuss more advantages that come with using this technique of studying proteins.

2.3 Change of Transmission during Trap

The resonance of the nanoaperture also assists in the detection of trapping events, since the transmission of the bow tie will change depending on the presence of a protein. This change in signal will be caused by a change in resonance wavelength of the aperture. A dielectic particle with a higher refractive index than water (> 1.33) being present in the aperture will increase (redshift) the resonance wavelength of the aperture.

The result of this change depends on the original situation. In case the resonance wavelength was originally lower than the laser wavelength, the redshift will cause the resonance to be closer to the laser wavelength, increasing the transmission of the aperture. If, however, the resonance wavelength was originally already higher than the laser wavelength, a further redshift will only increase the distance between the resonance peak and the laser wavelength. This causes a decrease in transmission intensity. This effect has been visualised in figure 6.

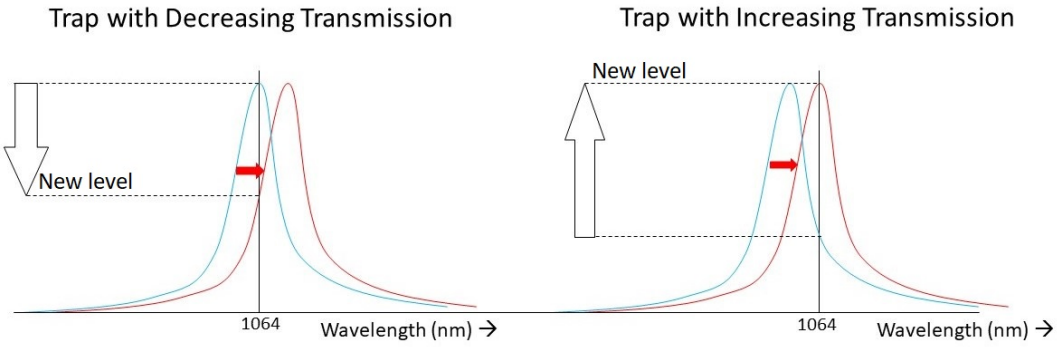

Figure 6: Visualised shift in resonance wavelength of the aperture in two cases. On the left, we see the decreasing case, where the redshift of the resonance peak moves it further away from the laser wavelength (1064nm), shown as the black vertical line. The dotted lines indicate the decrease in transmission. On the right, the increasing case is visualised, showing that the redshift moves the resonance peak closer to the laser wavelength, again in black. The increase in transmission that results is again indicated with the dotted lines.

A trapping event is clearly visible in the measured signal as a consequence of this phenomenon. Figure 7 shows what this looks like. When the trapping occurs, the signal cleary increases to a different level. We only see the signal return to its original state after the laser has been turned off for a while. This proves that the particle was actually trapped and not just stuck to the surface. An example of a particle that sticks to the surface can be found in the appendix.

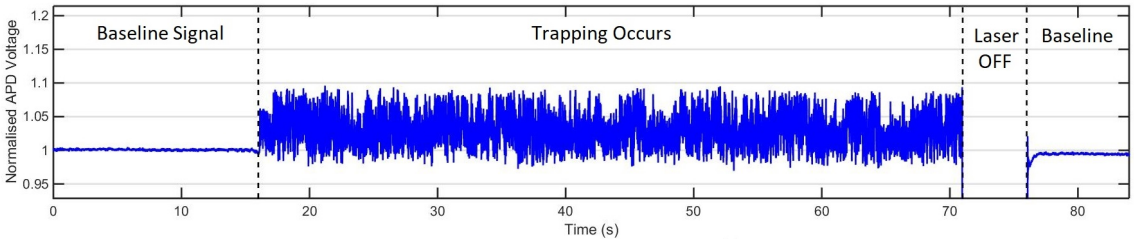

Figure 7: Normalised signal of the bow tie transmission as recorded by the APD. We notice that the signal changes significantly when a particle enters the trap. We see that the particle remains in the trapping region for as long as the laser remains turned on and only leaves when the laser has been turned off for a few seconds. We now see that we can create a stable trap for a time span in the order of a minute.

The advantage of this is that we can detect traps by recording the signal that is transmitted through the sample. Therefore, we do not need to label any of the proteins that we decide to use in experiments, unlike with techniques like FRET, which requires the biochemical modification of the proteins of interest. This removes another potential source of disturbance that can affect the way in which HSP90 undergoes its conformational change and makes this technique less invasive.

2.4 Heat Flow Model

We expect to cause less heating in the system, because we are able to use lower laser power. In this part, a model will be created to calculate the actual temperature when we use this technique. In this way, we can determine whether large amounts of thermal noise will still have to be taken into account and if the laser might cause particles in the trap to heat up significantly, which can also lead to altered behaviour of the studied proteins.

2.4.1 Laser Power Distribution

We start working on the model by making a few assumptions and then deriving the equation that governs the situation. First, we will make some assumptions about the laser beam. We assume the laser beam is roughly circular and is normally distributed: $I(r) = I_0 e^{-cr^2}$ with r the distance in the x,y-plane to the centre. I_0, the intensity of the beam in the centre, is a bit difficult to determine, but we can relate it to the total laser power by integrating:

$$P_{tot} = \int_0^\infty 2\pi r I_0 e^{-cr^2} dr = 2\pi I_0 \left[-\frac{1}{2c} e^{-cr^2} \right]_0^\infty = \frac{\pi}{c} I_0 \tag{2}$$

This results in $I(r) = \frac{cP_{tot}}{\pi} e^{-cr^2}$, which is convenient since the total laser power is known, as well as the scale of the width of the peak. Further, we assume that the bow tie does not exist. That is, the resonance effect caused by the bow tie is considered, but we do not consider its role in heat conduction. This is justified because the hole has the size in the order of 10 nanometers, while the laser beam has a diameter in the order of a micron. Apart from this, the situation is circularly symmetric and we therefore do not expect any heat to flow through $r = 0$, which significantly reduces the impact of the assumption.

2.4.2 Heat Equation

Now we derive the heat equation on this circular disk that we have. We choose an infinitesimally thin disk ring with radius r and thickness dr. The thickness in z-direction will be called h. The total internal energy can be expressed as:

$$E_{int}(r) = V(r)e(r) = 2\pi r dr h \rho c_v u(r) \tag{3}$$

Where ρ is the density, c_v the specific heat, both assumed constant throughout the gold object and $u(r)$ the temperature difference with the surroundings at distance r from the middle. The total change in internal energy in this disk is:

$$\frac{\partial E_{int}(r)}{\partial t} = 2\pi r h dr \rho c_v \frac{\partial u}{dt} = 2\pi r h q|_r - 2\pi (r + dr) h q|_{r+dr} + 2\pi r dr I(r) - 2\pi r dr S u \tag{4}$$

Where the first two terms signify influx and outflux by conduction, the third term is heating by the laser and the last term is convection to the surroundings. Rewriting the equation with $q = -\lambda \frac{\partial u}{\partial r}$ gives:

$$\begin{aligned} \frac{\partial u}{\partial t} &= \frac{\lambda}{\rho c_v} \frac{1}{r} \frac{(r + dr)\frac{\partial u}{\partial r}|_{r+dr} - r\frac{\partial u}{\partial r}|_r}{dr} + \frac{I(r)}{h\rho c_v} - \frac{S}{h\rho c_v} u \\ &= \frac{\lambda}{\rho c_v} \left[\frac{1}{r} \frac{\partial}{\partial r} \left(r \frac{\partial u}{\partial r} \right) + \frac{I(r)}{h\lambda} - \frac{S}{h\lambda} u \right] \end{aligned} \tag{5}$$

When we define $k \equiv \frac{\lambda}{\rho c_v}$ and split up the derivative with respect to r, we get

$$\frac{\partial u}{\partial t} = k \frac{\partial^2 u}{\partial r^2} + \frac{k}{r} \frac{\partial u}{\partial r} + \frac{k I(r)}{h\lambda} - \frac{kS}{h\lambda} u \tag{6}$$

We have two boundary conditions in the r-direction. First, we must have $u(r, t) \to 0$ when $r \to \infty$ since we want the temperature to approach the temperature of the surroundings. As a second boundary condition, we require that u is finite in $r = 0$. As an initial condition, we can take $u(r, 0) = 0$, meaning that the sample starts off with the temperature of the surroundings.

This is the specific form of the heat equation that will govern this situation. We see that the total change in temperature depends on the internal conduction (first and second term), heating by the laser (third term) and the convective transfer in the water surrounding the gold (fourth term).

2.4.3 Analytical Solution for the Stationary Situation

The laser remains turned on for a long time in preparation for the experiments so that it can stabilise. Therefore, we are only interested in the stationary situation. This means that $\frac{\partial u}{\partial t} = 0$, and we define $\tilde{S} \equiv \frac{S}{h\lambda}$ and $\tilde{I}(r) \equiv \frac{I(r)}{h\lambda}$. Since our PDE has now turned into an ODE, this gives us:

$$\frac{d^2 u}{dr^2} + \frac{1}{r} \frac{du}{dr} + \tilde{I}(r) - \tilde{S} u = 0 \tag{7}$$

Which we can rewrite to

$$\left(\frac{d^2}{dr^2} + \frac{1}{r}\frac{d}{dr} - \tilde{S}\right) u = -\tilde{I}(r) \tag{8}$$

This brings us no closer to solving the equation, but it is an interesting result. We see that the left-hand side is a linear operator working on u, while the right hand side is linear with the laser power we apply. From this we can see that increasing the laser power will increase the temperature in the stationary situation by the same factor, whatever distribution we will end up finding. We can use this result later for checking our final result for u.

The right hand side is also the part that makes this equation inhomogeneous. We will solve the homogeneous solution first, after rewriting it into a form that is familiar:

$$r^2\frac{d^2u_h}{dr^2} + r\frac{du_h}{dr} - r^2\tilde{S}u_h = 0 \tag{9}$$

This is a form of the Bessel Equation, which results in the homogeneous solution:

$$u_h(r) = c_1 I_0(\sqrt{\tilde{S}}r) + c_2 K_0(\sqrt{\tilde{S}}r) \tag{10}$$

Where I_0 and K_0 are the Modified Bessel Functions of the first and second kind, respectively. We now proceed to find the solution to our problem. According to our model we choose $\tilde{I}(r) = \frac{I_0}{h\lambda}e^{-cr^2}$. To avoid an overly complicated expression we define $B \equiv \frac{I_0}{h\lambda}$. Now, when we solve for equation 7, we get:

$$\begin{aligned} u(r) = c_1 I_0(\sqrt{\tilde{S}}r) + c_2 K_0(\sqrt{\tilde{S}}r) + I_0(\sqrt{\tilde{S}}r)\int_1^r \left[\frac{B}{2}e^{-cx^2}\pi x K_0(\sqrt{\tilde{S}}x)\right]dx + \\ K_0(\sqrt{\tilde{S}}r)\int_1^r \left[-\frac{B}{2}e^{-cx^2}\pi I_0(\sqrt{\tilde{S}}x)\right]dx \end{aligned} \tag{11}$$

Our boundary conditions require the solution to be finite in $r = 0$ and when $r \to \infty$. In order to satisfy this, we must choose

$$c_1 = \frac{B}{2}\int_0^1 e^{-cx^2}\pi I_0(x)dx \tag{12}$$

$$c_2 = -\frac{B}{2}\int_1^\infty e^{-cx^2}\pi x K_0(x)dx \tag{13}$$

We see that each term is now linear with B, which is what we predicted from equation 8. We also notice that this expression is very complicated, making it difficult to create a plot or to do calculations with. We will therefore also create a numerical model of the situation, in order to get an approximation for the stationary solution.

2.4.4 Numerical Approximations

In order to numerically work out this situation, we start with an array u, containing the temperature values on $0 < r < R$, where R is a radius at least 10 times the width (at half height) of the laser peak. At $t = 0$, we start with $u = 0$, so the entire surface has the temperature of the surroundings. For each time step Δt, we calculate a value for the right hand side of equation 6 for each point in the vector $\vec{r} = [r_1, ..., r_N]^T$, with $r_N = R$, multiply it with the time step and and add it to u. In order to calculate this, we have to discretise the derivatives in the equation. We choose:

$$\frac{\partial^2}{\partial r^2} = \frac{1}{\Delta r^2}\begin{bmatrix} -2 & 2 & 0 & \dots & 0 \\ 1 & -2 & 1 & \ddots & \vdots \\ 0 & \ddots & \ddots & \ddots & 0 \\ \vdots & \ddots & 1 & -2 & 1 \\ 0 & \dots & 0 & 1 & -1 \end{bmatrix} \quad \frac{\partial}{\partial r} = \frac{1}{\Delta r}\begin{bmatrix} -1 & 1 & 0 & \dots & 0 \\ 0 & -1 & 1 & \ddots & \vdots \\ \vdots & \ddots & \ddots & \ddots & 0 \\ 0 & \dots & 0 & -1 & 1 \\ 0 & \dots & 0 & 0 & 0 \end{bmatrix} \tag{14}$$

These are approximations based on $\frac{d^2u_n}{dr^2} \approx \frac{u_{n-1}-2u_n+u_{n+1}}{\Delta r^2}$ and $\frac{du_n}{dr} \approx \frac{u_{n+1}-u_n}{\Delta r}$. At the boundary $r = 0$, we remark that the situation is circularly symmetric, so that $u_{-1} = u_1$. At the boundary $r = R$, we choose to model it as an insulated surface, so we say $u_{N+1} - u_N = 0$, resulting in $\frac{d^2u_N}{dr^2} = \frac{u_{N-1}-u_N}{\Delta r^2}$ and $\frac{du_N}{dr} = 0$, which is typical for an insulated boundary. If this insulation assumption is not justified, then there must still exist a temperature gradient at $r = R$. In that case we should increase R, not change the assumption, since we want to model this situation so that all heat is dissipated by convection.

The next step is finding the right values for all of the parameters. The calculation of the parameters is based on data from the Transport Phenomena Data Companion by Janssen and Warmoeskerken [7]. The calculations and resulting values can be found in the Appendix.

2.4.5 Stability Analysis

For finding the numerical solution to the differential equation, we will use the Euler Forward method. This means that for each time step, we will calculate $u_n^{t+1} = u_n^t + f_n(u,r)\Delta t$. In our case, the function f is a function of the numerical approximations to the derivatives defined above, of r and of a couple of constants. Using equation 6, we can define:

$$f_n(u,r) = \frac{k}{\Delta r^2}(u_{n+1} - 2u_n + u_{n-1}) + \frac{k}{r\Delta r}(u_{n+1} - u_n) + \tilde{I}(r) - \tilde{S}u_n \tag{15}$$

If we assume an initial distribution $u_n^t = \cos(\pi n) = (-1)^n$, which is the highest possible wave number that can exist for a chosen value of dr, then we can calculate:

$$f_n(u,r) = \frac{-4k}{\Delta r^2} + \frac{-2k}{r\Delta r} + \tilde{I}(r) - \tilde{S} \tag{16}$$

$$\geq \frac{-6k}{\Delta r^2} + \tilde{I}_0 - \tilde{S} \tag{17}$$

Because $f_n(u,r)$ is smallest at $n = 1$, since there $r = \Delta r$, and for other points $r > \Delta r$. For stability, we must now make sure $|f_n(u,r)\Delta t + 1| \leq 1$ [21], so

$$\left(\frac{-6k}{\Delta r^2} + \tilde{I}_0 - \tilde{S}\right)\Delta t \geq -2 \tag{18}$$

$$\left(\frac{6k}{\Delta r^2} - \tilde{I}_0 + \tilde{S}\right)\Delta t \leq 2 \tag{19}$$

$$\Delta t \leq \frac{2}{\frac{6k}{\Delta r^2} - \tilde{I}_0 + \tilde{S}} \approx \left(\frac{3k}{\Delta r^2} + \frac{\tilde{S}}{2}\right)^{-1} \tag{20}$$

This last approximation is based on the fact that $1/\Delta r^2$ and $\tilde{S}$ are very large terms when entering realistic values, while $\tilde{I}_0$ is not. We now have a maximum time step for our integration. With the realistic values entered, this results in a maximum Δt of around $4.3 \cdot 10^{-15} s$. When testing this is the model, we see that it is very close to the maximum value. From $4.6 \cdot 10^{-15} s$ the model starts to diverge, as can be seen in figure 8. We therefore conclude that our estimate of the stability condition is very close to the actual value.

We are able to estimate this value so accurately, because we know which point will be the most sensitive to a larger time step: the point $n = 1$. This is where $r = \Delta r$ and where our model will start to diverge first. We also see this happen if we look at figure 8, since the distribution will always converge to 0 when r becomes large, no matter how much it oscillates near $r = 0$.

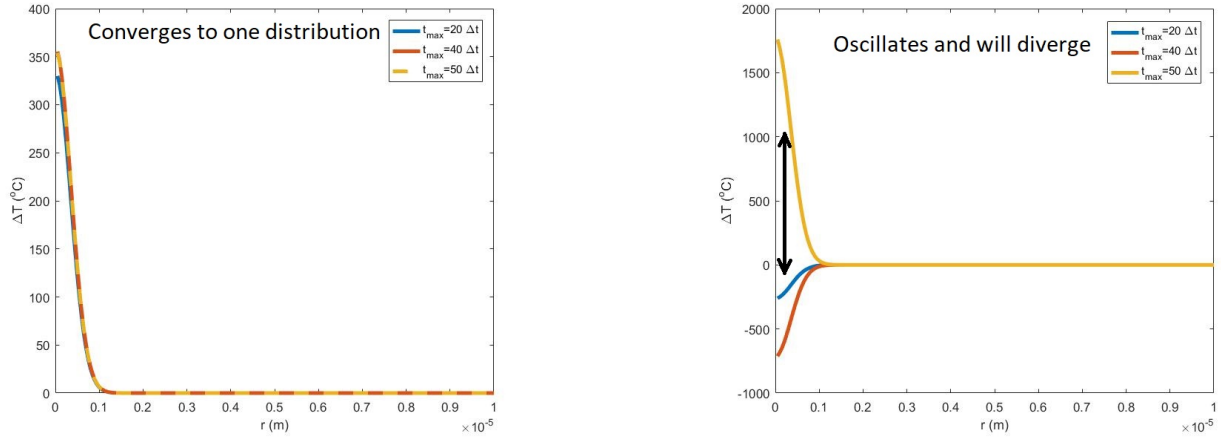

(a) $\Delta t = 4.3 \cdot 10^{-15} s$ (b) $\Delta t = 4.6 \cdot 10^{-15} s$

Figure 8: The results of the heat flow model for $\Delta t = 4.3 \cdot 10^{-15} s$ (left) and for $\Delta t = 4.6 \cdot 10^{-15} s$ (right). The blue, red and yellow lines are the distributions after 20, 40 and 50 time steps respectively. We see that the left graph converges to a constant distribution and the right graph oscillates and diverges. We also see that the divergence happens for r near the 0 boundary, never near the other boundary.

2.4.6 Results

The model is run for a laser power of 20mW, which is the value with which the HSP90 proteins will be trapped. The nanoaperture can increase the electric field in the area at least 20-fold. Therefore, the model is also run for a 20 times laser power, which would be needed to achieve the same trapping force without the nanoaperture. The results of the model are displayed in figure 9.

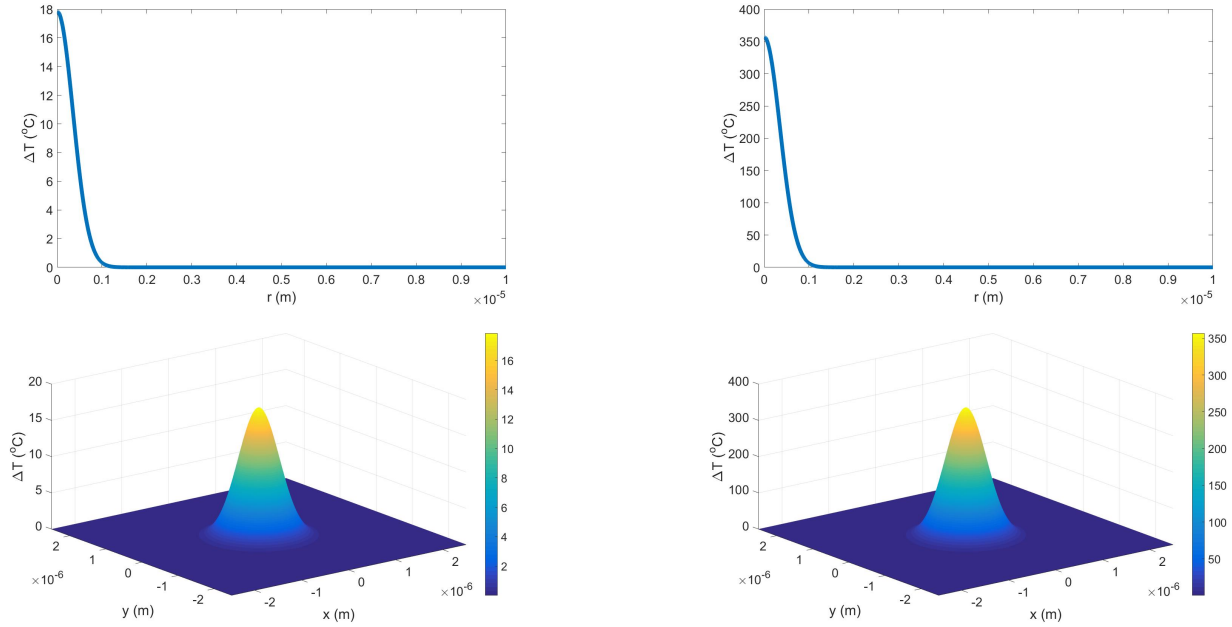

(a) $P_{tot} = 20mW$ (b) $P_{tot} = 400mW$

Figure 9: The final results of the Heat Flow Model. We see the resulting temperature differences with the surroundings. Both results show roughly the same temperature distribution. At 20mW, the maximum temperature increase is roughly 18^oC and at 400mW, it is over 350^oC. This leads us to the conclusion that the used setup limits the temperature increase to a level that is within an acceptable range to study HSP90.

We see that the temperature increase can be limited significantly using the resonance of the nanoapertures. The temperature increase is reduced from 350^oC to about 18^oC. First of all, we conclude that the resonance is essential to keep HSP90 from denaturing, which happens slightly above 50^oC [4]. This is important for this research because we want to avoid changing the protein properties during measurements. Furthermore, we conclude that the sample will not melt using this shape of antenna. Lastly, we see now that the temperature increase will not lead to very violent fluid flows that can disturb the situation, like an increase of 350^oC could. Note: this result complies with the observation we did in equation 8 that increasing the laser power would result in an increase in temperature with the same factor. This is confirmed now we see that both have increased with a factor 20.

2.5 3D Random Walk

In order to check whether the trap is expected to be stable, we can run a small simulation of a particle in the force field that results from the electric field gradient force.

2.5.1 Brownian Motion in Force Field

The model we will create will be based on the concept of Brownian Motion. The simplest way to model this is by choosing a random direction each time step, assuming an average velocity caused by thermal energy and adding this step to the original position.

$$\mathbf{x}_{n+1} = \mathbf{x}_n + \bar{v} \cdot \hat{\mathbf{r}} \cdot \Delta t \tag{21}$$

In 2D, we can choose a random angle $0 \leq \phi < 2\pi$, and choose $\hat{\mathbf{r}} = (\cos\phi, \sin\phi)^T$ in order to have no average velocity.

If we would like to add a force field to this, that would not be very straightforward. A force causes a change to the velocity of a particle each time step, not just a change in its position. This requires a certain inertia, which does not yet exist in this model. We will change our model to allow a force to act on the particle.

For this change, we will assume a particle that takes its position with it to the next time step, like the one before, but also its velocity, unlike the one before. For the position we will define $\mathbf{x}_{n+1} = \mathbf{x}_n + \mathbf{v}_n \cdot \Delta t$, and for the velocity $\mathbf{v}_{n+1} = \mathbf{v}_n + \bar{a} \cdot \hat{\mathbf{r}} \cdot \Delta t$, where $\hat{\mathbf{r}}$ is still the random direction in 2D.

Now we have to find some way to get a good estimate for the average acceleration. We can estimate this as follows: we start by assuming that in the last time step, the Δx was in the $-x$-direction. The situation in circularly symmetric and we are only estimating the magnitude now, so this is allowed. This means that $v_n = -\bar{v}\hat{x}$, but choosing any other direction would yield exactly the same result. For the next time step, the velocity will have the same magnitude, but will be in a random direction. The change in velocity during this time step Δt is therefore $\Delta\mathbf{v} = \bar{v}(1 + \cos\phi, \sin\phi)^T$. The average magnitude can be calculated by integrating over the angles ϕ:

$$|\Delta\mathbf{v}| = \frac{\bar{v}}{2\pi}\int_0^{2\pi}\sqrt{(1+\cos\phi)^2 + \sin^2\phi}\,d\phi = \frac{\bar{v}}{2\pi}\int_0^{2\pi}\sqrt{2+2\cos\phi}\,d\phi = \frac{\bar{v}}{\pi}\int_0^{2\pi}|\cos(\phi/2)|d\phi \tag{22}$$

We split up the integral and get:

$$|\Delta\mathbf{v}| = \frac{\bar{v}}{\pi}\left[\int_0^{\pi}\cos(\phi/2)d\phi - \int_{\pi}^{2\pi}\cos(\phi/2)d\phi\right] = \frac{2\bar{v}}{\pi}\left[\sin(\phi/2)|_0^{\pi} - \sin(\phi/2)|_{\pi}^{2\pi}\right] = \frac{4\bar{v}}{\pi} \tag{23}$$

Since this is the average magnitude of the velocity change during time Δt, we can add $\frac{4\bar{v}}{\pi} \cdot \hat{\mathbf{r}}$ to the velocity each time step. Now that we have introduced the concept of inertia into the model, we can also add a force term. The total change in velocity per time step now becomes:

$$\mathbf{v}_{n+1} = \mathbf{v}_n + \frac{4\bar{v}}{\pi}\hat{\mathbf{r}} + \frac{\mathbf{F}}{m} \tag{24}$$

Integrating this for each time step will yield the path of the particle.

2.5.2 Spatial Boundaries

In the (x,y)-plane, the trap area is shielded by the bow tie structure. The bow tie is modelled as can be seen in figure 10. We will assume the particle will bounce off the boundary elastically. If the particle exceeds the boundary in the x-direction, its velocity in the x-direction can just be mirrored. In the y-direction, the boundary is modelled by a tilted line, $y = \pm cx$, depending on which part we are looking at. This means the direction perpendicular to the line is $\hat{\mathbf{n}} = (\mp c, 1)^T$, and we should mirror the velocity vector in this direction. We can do this by:

$$\mathbf{v}_{n+1} = (\mathbf{v}_n - \text{proj}_{\hat{n}}\mathbf{v}_n) - \text{proj}_{\hat{n}}\mathbf{v}_n = \mathbf{v}_n - 2\text{proj}_{\hat{n}}\mathbf{v}_n \tag{25}$$

Where the projection is defined as $\text{proj}_{\mathbf{a}}\mathbf{b} = \frac{\mathbf{b}\cdot\mathbf{a}}{||\mathbf{a}||^2}\mathbf{a}$. This leads to the results shown in figure 10. We see that the particle does indeed bounce off the boundaries as we were trying to achieve.

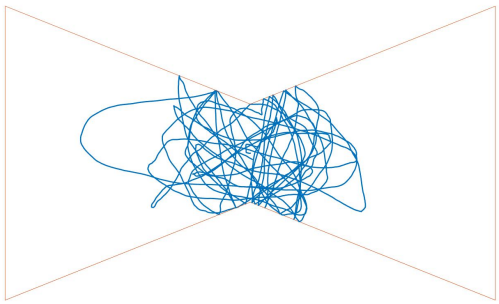

Figure 10: Random walk generated with the concepts described before. The shape of the bow tie is indicated in red, the particle trace is shown in blue. We see that the particle does indeed bounce on the boundaries.

2.5.3 Changing to 3D

Changing the model to 3D is more complicated than just adding a third value to each vector that we are using. A significant change we have to make, is the way in which the random direction is generated. Where we did this with a random angle between 0 and 2π in the 2D case, we need two angles when considering the 3D case. ϕ will still be our angle in the (x,y)-plane, and θ will be the angle relative to the positive z-axis, just as regular spherical coordinates are defined, so that $x = r\sin\theta\cos\phi$, $y = r\sin\theta\sin\phi$, $z = r\cos\theta$.

Generating a random direction is a little more difficult. The angle ϕ can still be chosen randomly between 0 and 2π, but we cannot do the same for θ if we want a homogeneous distribution. This is because the surface area of a sphere covered by a change $d\theta$ depends on θ. This weight is proportional to $\sin\theta$, since all the points that correspond to a certain θ lie on a circle with circumference $2\pi r\sin\theta$. Figure 12 shows the result of randomly generated points with a homogeneous distribution of θ. Figure 11 shows how the projections have been made. We see that the concentration near the top and bottom is higher than around the rest of the sphere.

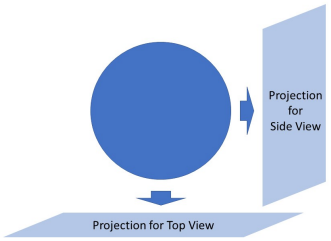

Figure 11: The way in which the scattered sphere is projected for obtaining the plots in figure 12

(a) Standard θ (Top view) (b) Standard θ (Side view) (c) Adjusted θ (Top view) (d) Adjusted θ (Side view)

Figure 12: Scatter plots of homogeneous θ distribution and of the arcsine adjusted θ distribution. (a) and (c) show the x,y-plane (sphere from the top), whereas (b) and (d) show the x,z-plane (sphere from the side). We see that the homogeneous θ distribution yields a scatter plot that is denser at the top and at the bottom, while the adjusted version yield a scatter plot that is homogeneously distributed over the surface of the sphere.

We should therefore convert our randomly generated function by taking the arcsine, since this is the inverted function of the cumulative distribution function. We should, however, input a number between -1 and 1. Then the arcsine will return a number between $-\pi/2$ and $\pi/2$. The final function for our randomly generated θ will therefore become: $\theta = \arcsin(2\text{rand}(\,) - 1) + \pi/2$, where rand( ) is the MATLAB function that generates a random number between 0 and 1. This result has also been shown in figure 12. We see that the scattered points are now equally distributed over the sphere.

2.5.4 Results

When we implement this in the model, we generate an array of points in $\mathbb{R}^3$ that signifies the path of our particle. The loop will terminate if the particle crosses a boundary in the z-direction, which we define at 10 nm away from the plane of the bow tie. This results in the path shown in figure 13. We see that the termination turns out not to be necessary in the 3 seconds that the loop is running, and the particle stays quite close to the middle of the trap.

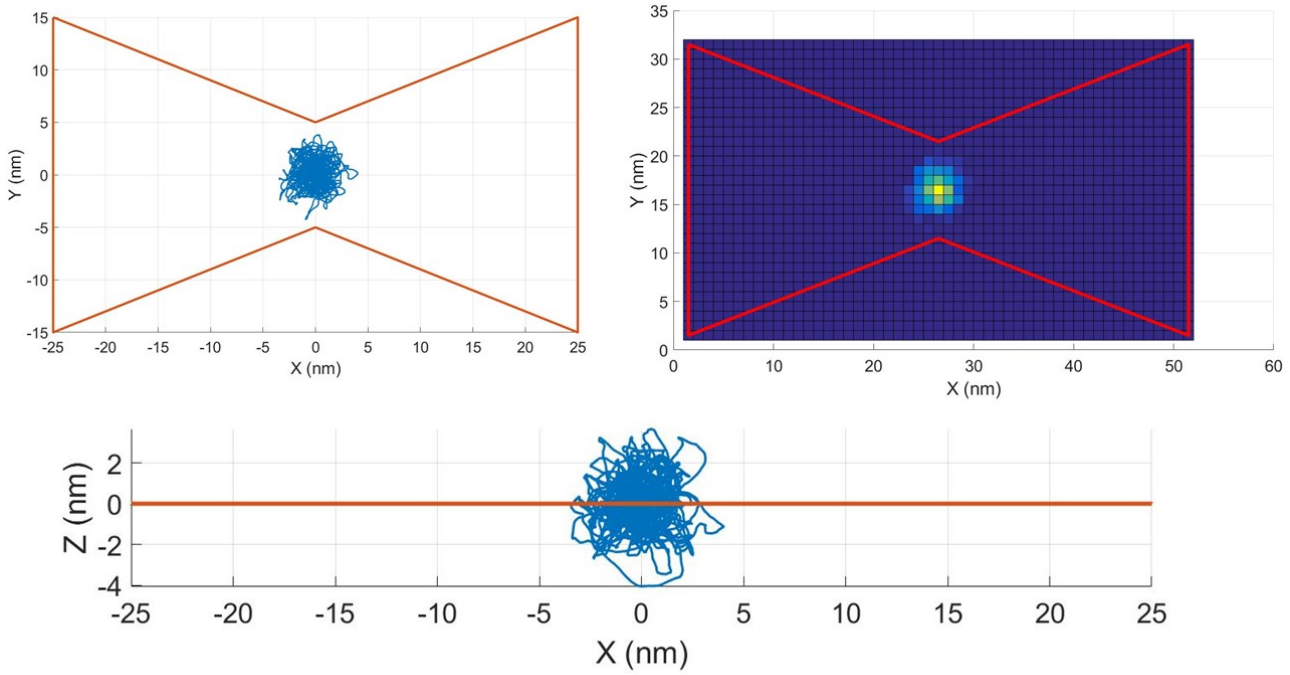

Figure 13: Random walk in three dimensions with a running time of 3s. The top left and the bottom image show scatter plots of the particle. The top right image shows a heat map of where the particle has been. We see that the loop has been able to finish the 3 seconds and a termination due to drift outside the structure was not necessary.

2.6 Summary of Theoretical Background

From methods like FRET and Cryo-EM, we know that HSP90 undergoes a conformational change. We have seen that dielectric particles can be trapped optically and that inverted bow tie shaped nanoapertures amplify the electric field of a laser beam so that we can use it for stronger optical trapping. We then showed that the transmission of a nanoaperture changes during a trapping event, allowing us to directly measure the trapped particles, which removes the need for labelling. After building models to simulate the heat flow and a random walk, we concluded that the laser heating would be limited to around 18^oC above room temperature, so below the denaturation temperature of HSP90 ($> 50^oC$)[4], while still creating a very stable trap. We will now continue to describe how the actual trapping experiments were set up.

3 Experimental Methods

In this section, the methods for obtaining, processing and analysing the data will be described. The experimental setup will be explained, as well as how the structures are created in practice. Multiple ways of analysing the data are illustrated.

3.1 Experimental Setup

The setup used is shown in figure 14. The setup starts with a laser, generating the 1064nm beam. This beam is collimated, filtered and polarised. This lets us control the laser power using a single motor, without actually having to change the laser current. The beam then passes through two half-wave plates with which the polarisation of the beam can be controlled. With several mirrors, it is aimed at the objective and through the sample, after which the transmission is recorded using the APD. A photo of the setup is included in the appendix.

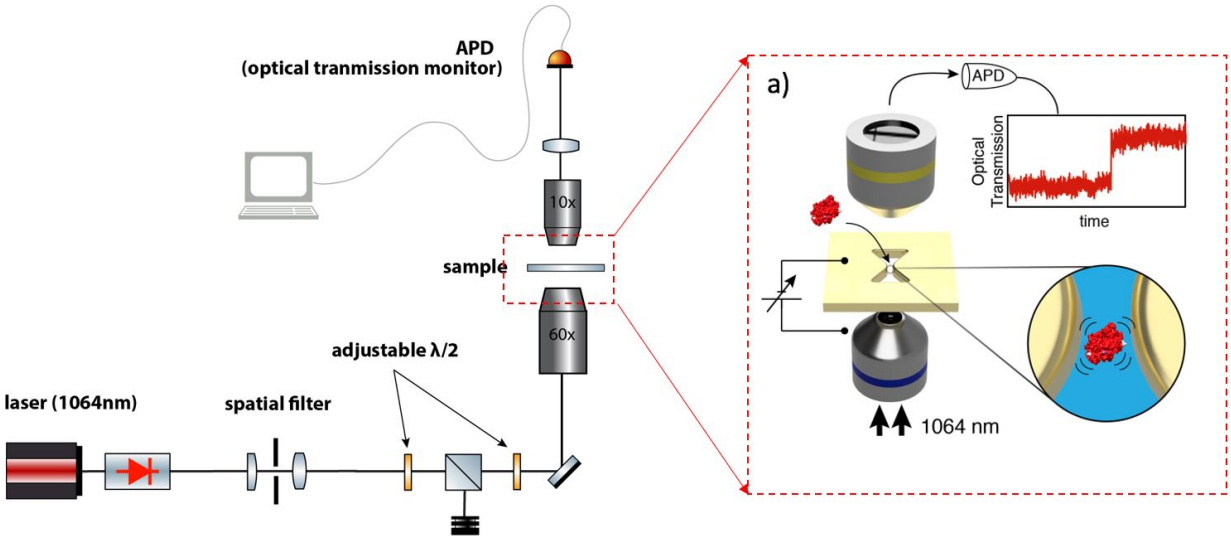

Figure 14: Setup used for conducting the experiments. Reproduced from [20]. The laser is collimated, spatially filtered and polarised. The rotation of the polarisation can be controlled. The beam passes trough the objective lense and the sample. Then, the APD collects the resulting signal on the other side of the sample after magnification. Photos of the actual setup can be found in the appendix.

During the time when the experiments were run, we experienced multiple issues with an unstable baseline and interference from outside the setup. In order to minimise the impact of these disturbances on the results, we took several measures which improved the stability. For a start, we put metal weights in the curtains to keep air flows in the lab from disturbing the laser beam. We then put metal covers around the part where the sample was mounted, to also shield this part from being affected by the turbulence in the air. As a final measure, we increased the temperature of the room in the central control system to around 21^oC. This was an important change, since the air conditioning in the lab cooled the room down by interchanging periods of rapid cooling with stretches of not cooling at all. By increasing the temperature, it did not have to do this as often or as intensely, significantly reducing the amount of drift that the baseline showed. An example of a trace with a lot of drift can be found in the appendix.

3.2 Fabrication of Structures and Components

Before etching the holes, a membrane is created from silion nitide (SiN), coated on a piece of a silicon wafer. The entire surface gets a very thin layer of gold coating (100nm). Then, the bow tie shaped holes need to be etched into this membrane. The holes are created using Focused Ion Beam (FIB) milling. In one sample, 4 sectors are created with 16 bow ties each. The spatial properties are constant within each sector, but can differ over the different sectors within one sample. Differences within one sector are caused by variations inherent to the FIB machine, but these remain very small, since the maximum variation is $< 1nm$.

When the structures have been created, they can be inspected using a transmission electron microscope (TEM). In this way, their quality and actual size can be checked. The spatial dimensions affect the resonance frequency and the trapping potential of a bow tie. Figure 15 shows the created bow ties in an electron microscope.

When the structures have been fabricated, we need a good way to lead the protein solutions to the membrane. For this, a combination of flow cells is used. The main part is made of PEEK (polyether ether ketone). The smaller channels, however, are created by moulding PDMS (polydimethylsiloxane) into the right shape.

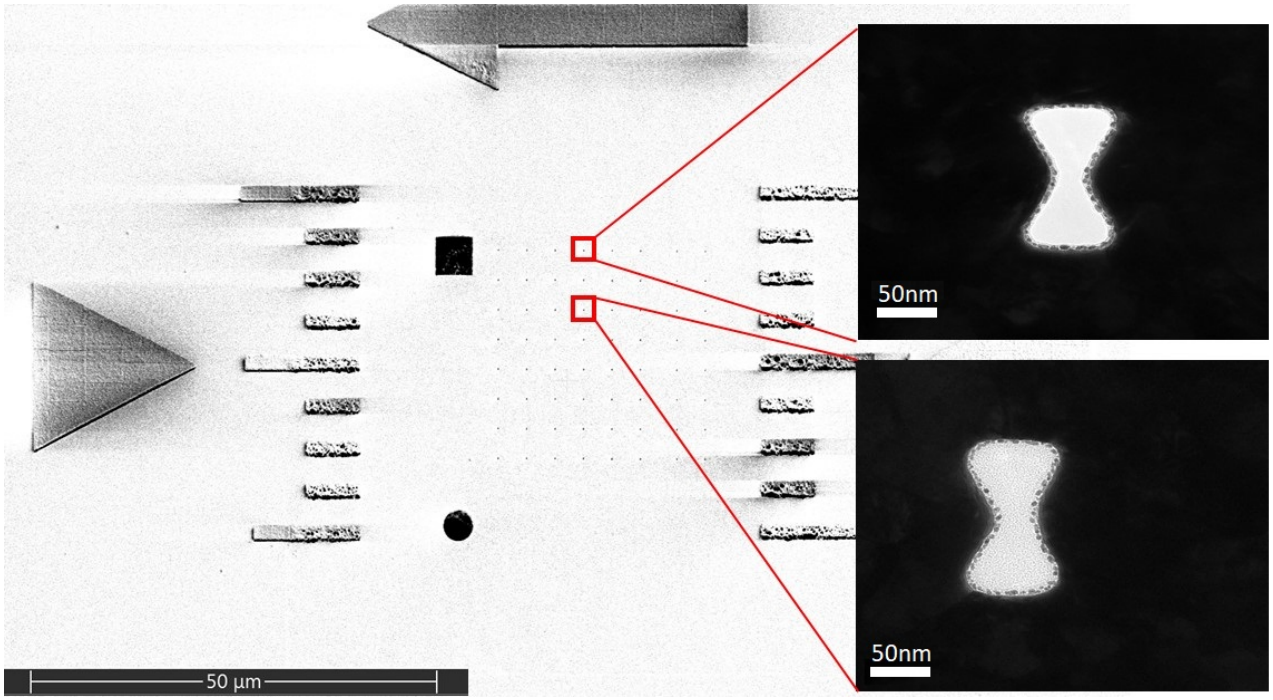

Figure 15: The result of the FIB milling process. Two bow ties have been enlarged. We also see two apertures, one square and one circle. These are used for aligning the laser and for orientation, so that it is always clear which bow tie is being inspected. All other visible features on the gold surface are used for orientation and calibration when preparing the measurements.

3.3 2D Maps of Sample Surface

Theoretically, we know that the laser signal will resonate in the nanoapertures using the right polarisation, but we want to verify this experimentally. In order to do this, we take two '2D maps' of the surface. A 2D map is obtained by moving the laser over the entire surface and recording the resultant transmission through it. This yields a 2D surface of intensities recorded. This 2D map is taken twice: once with polarisation that should resonate and once with a polarisation that is exactly orthogonal to this direction. In this way, we can check that the increase in transmission is because of resonance and not simply because of the fact that there is a hole in the plate. Figure 16 shows the two 2D maps side by side. From the figure, we can clearly see that the transmission for one polarisation direction is much larger than with polarisation in the perpendicular direction. From this, we can tell that the bow tie structures show resonance close to the laser frequency.

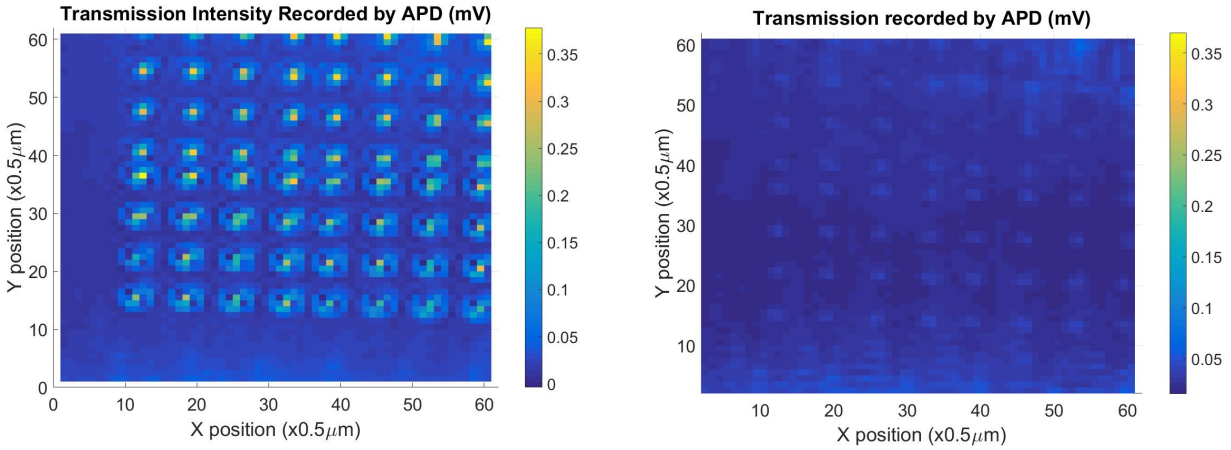

(a) Polarisation Parallel with Resonance Direction

(b) Polarisation Orthogonal to Resonance Direction

Figure 16: 2D Maps of the membrane surface with different polarisations. Note the scales on the right of the plots: we see that the bow ties become very clear with the right polarisation, but are hardly visible in the noise with the orthogonal polarisation. We can now conclude that the bow ties do indeed resonate with a wavelength close to the laser light.

3.4 Control Tests

The goal of the experiments is demonstrating whether conformational changes in HSP90 can be visualised with this technique of optical trapping. In order to achieve this, we must record signals for trapped HSP90 proteins alongside signals for trapped objects that certainly do not show any conformational changes. In this way, we can distinguish the conformational changes from other influences on the measured signal. The method we will most frequently use during the experiments is comparing our results to the results of the same experiment, which is run with polystyrene (PS) beads instead of proteins. The PS beads resemble the HSP90 proteins in the sense that they are small pieces of a dielectric material floating around in solution.

We expect these beads to behave roughly the same under trapping conditions as the HSP90 proteins, except without a conformational change. The beads have a diameter of roughly 20nm, which is quite a large difference with the 10nm size of the HSP90 proteins, and we should keep it in mind while discussing the experimental results. Still, the PS beads should work fine with the setup, since most of the bow ties have a gap size larger than 20nm. The gap is defined as the distance between the two sides of the bow tie exactly in the middle. Also, the electric field gradient exerts the same force on each piece of volume from equation 1, so the larger inertia is compensated by an increase in strength of the force.

Throughout the experiments, the sample is also tested regularly by looking at the bow tie transmissions when immersed in an 'empty' solution, meaning one without beads or protein, but only deionised water or only PBS (phosphate-buffered saline) solution. We do this to check that we do indeed not see any trapping events. This is to check that we are actually looking at trapping events from the beads or proteins, not an effect caused by the setup itself.

3.5 Signal Processing and Analysis

The signal that results from the setup is recorded using the APD. The data are processed using a labview program and can be viewed in the 'Transalyser' MATLAB code. The obtained data can be analysed in numerous ways. The following is an overview of the methods used in this project.

3.5.1 Bin Diagrams

One possible method to distinguish different states of the protein, is creating histograms of the obtained signal. Figure 17 illustrates the way in which information is extracted from the signal by putting the data from the Y-axis in a histogram. In this way, we can easily distinguish the baseline from the signal during the trap, and the distribution of the latter can tell us something about what is happening inside the bow tie. The baseline is represented by a very sharp peak, resulting from the fact that the baseline is very stable. The more chaotic behaviour of the trapping signal results in a much wider distribution of the trapping signal.

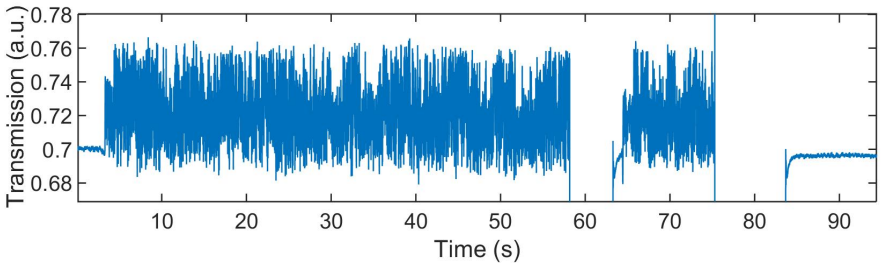

(a) Trapping Signal

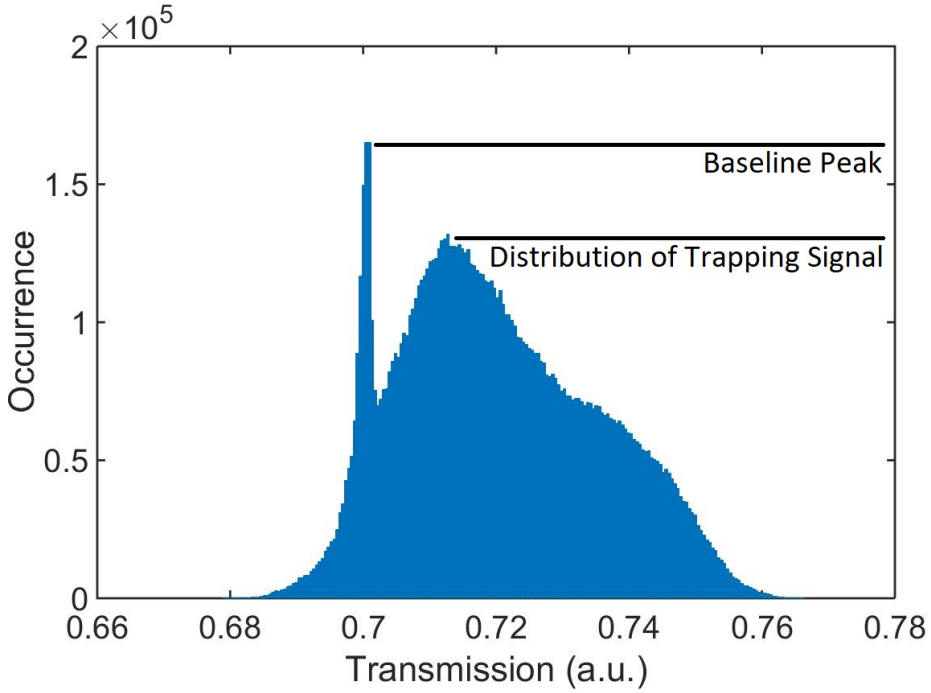

(b) Associated Histogram

Figure 17: Trapping signal with associated histogram showing the distribution of the signal over the y-axis. The histogram creates several bins and counts the occurrence of those levels in the signal. In figure (a), we notice the baseline is located at 0.7. In (b) we see that this results in the sharp peak at the same level. The rest of the distribution signifies the distribution of the signal in the trapped state.

3.5.2 Signal Correction

The setup is subjected to many different sources of noise from the environment and from parts of the setup itself. One common disturbance turns out to be a drift of the signal, which turns up in both baseline and trapping signal. Possible causes of this type of noise include turbulent fluid flows and vibration. Whatever the cause, correcting for the drift is essential for creating useful bin diagrams. If we don't do this, a horizontal signal would not create a sharp peak as it should, but would be smeared out over the y-axis, creating a broad distribution. On top of this, it can become very difficult to distinguish different parts of the signal from each other. Figure 18 shows the importance of correcting a signal, by comparing the histogram from an uncorrected and a corrected signal. We applied a simple linear correction to account for the drift in the baseline.

We can tell from the figure that directly creating a histogram from the signal causes a very unclear bin diagram. Both the effects of spreading out what should be a peak and different parts of the signal coinciding can be seen in the figure. It also becomes clear from the figure that this correction is not perfect yet. The peak generated by the base line is clearly not very sharp as a result of drift in the signal. When discussing the results, we will go into more detail of whether there still is a problem and, if so, what to do about it.

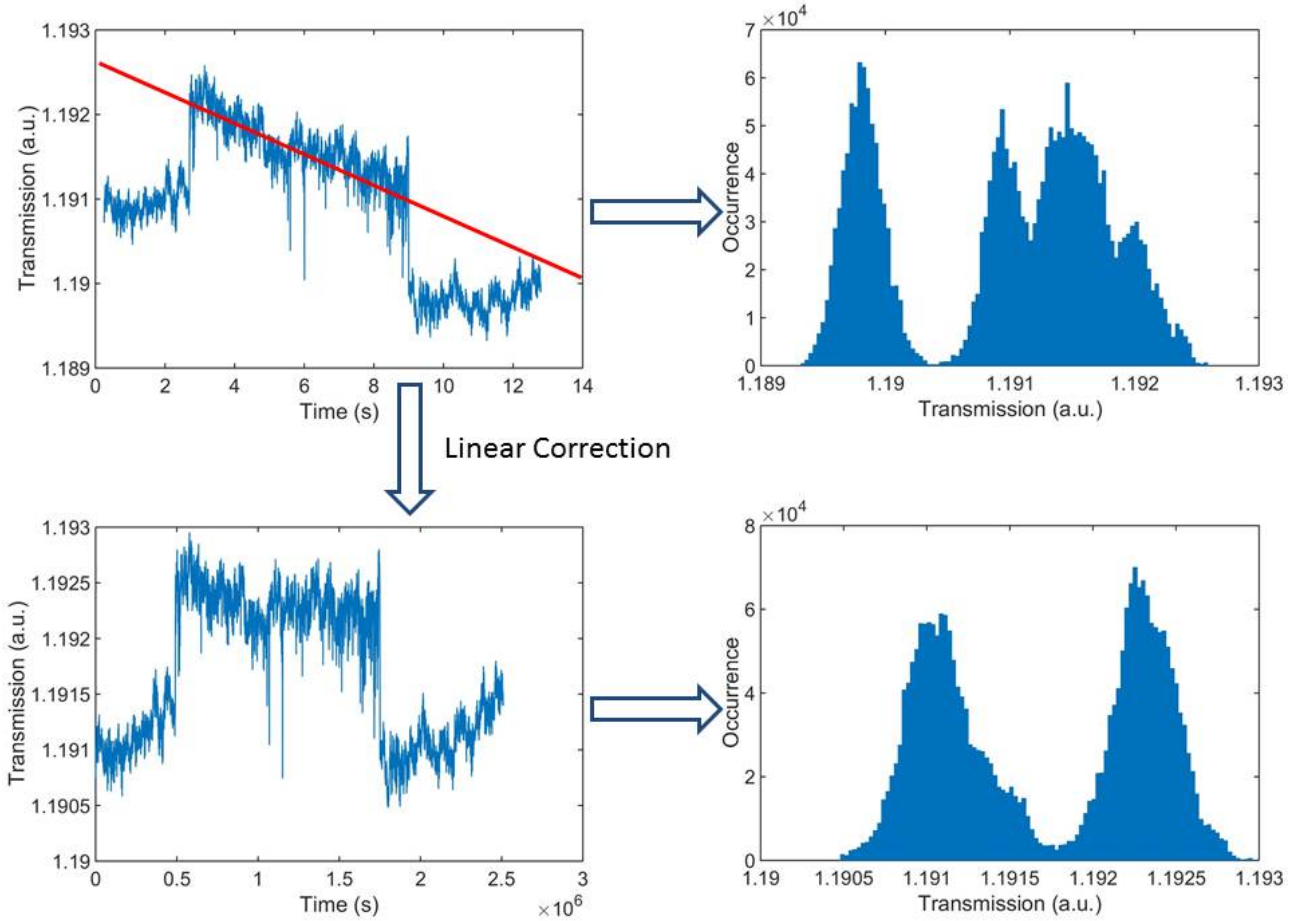

Figure 18: Histograms from an uncorrected (top left) and a corrected trace (bottom left). We see that the histogram of the uncorrected trace (top right) is confusing. The baseline has drifted during the trapping event, creating two separate base line peaks, one of which coincides with the trapping signal. The histogram created from the corrected signal (bottom right) shows two clearly distinguishable peaks, the one on the left resulting from the baseline, the one on the right from the trapping time.

3.5.3 Filtering the Signal

The measured signal is a result of many influences from many different sources. In order to successfully visualise the signal of interest, the signal that results from the conformational change, we must try to filter out all other influences. It is known from literature that the conformational changes take place with a frequency up to 1Hz [9]. When looking at the signal, it is interesting to explore what happens when we apply a low-pass filter to the signal. We hypothesize that we will obtain more information about the existence of a conformational change when we compare the filtered signals from trapped HSP90 and trapped beads, since we expect the signals to contain a lot of high frequency noise and interference.

Figure 19 illustrates the effects of filtering the signal of a trapped bead. This figure shows us that most of the original signal was indeed made up of high frequencies, since what remains after filtering strongly resembles a step function. The corresponding histogram shows nothing but two sharp peaks. As in the signals before, the left peak represents the baseline and the right distribution corresponds with the trapping signal. According to our hypothesis, the HSP90 should not behave in the same way when filtered like this. We expect the conformational change to take place in the domain below 1Hz, which means it should not be filtered out a low-pass filter of 10Hz.

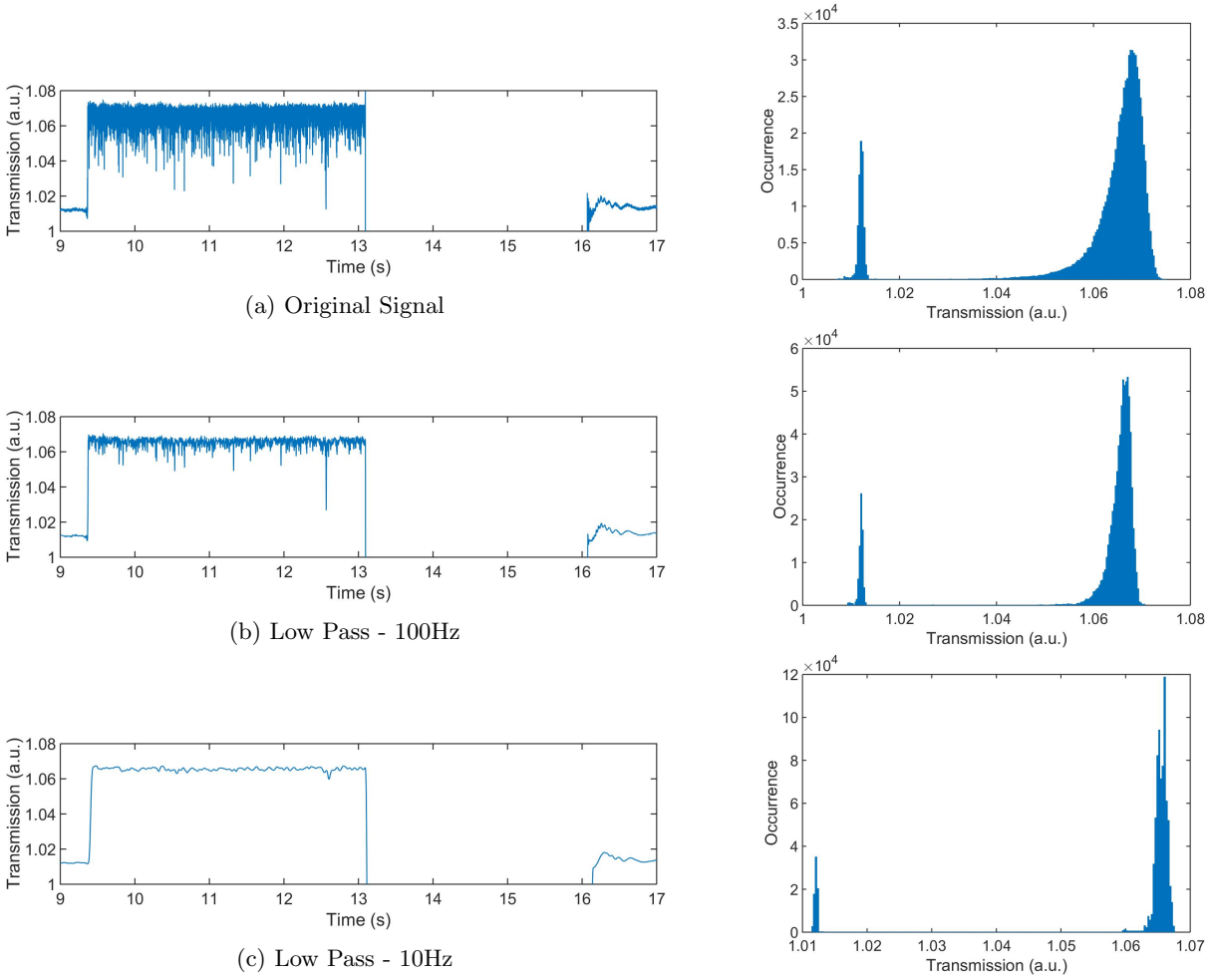

(a) Original Signal

(b) Low Pass - 100Hz

(c) Low Pass - 10Hz

Figure 19: The signal of a trapped bead with histogram of y-values. Subfigure (a) shows the original signal, which contains the signal domains that have been discussed earlier: the baseline, a trap, the laser being turned off and finally, a return to baseline when the laser is turned back on again. Subfigures (b) and (c) show what the result looks like after a 100Hz and 10Hz low-pass filter respectively. All histograms show a small baseline peak on the left and trapping signal peak on the right. What results after filtering is a signal that looks like a step function and a histogram with two sharp separate peaks. This shows us that the trapping signal barely contains any low frequencies. This is a good sign when trying to study the conformational change in HSP90, since we want other effects to be visible as little as possible when looking at the spectrum below 10Hz.

3.5.4 Power Spectrum Density

Another way of obtaining information from the signals that will be analysed, is by inspecting the power spectrum density (PSD). This can possibly give us more insight into what effects are at play, which would give us the possibility to filter out sources that are not of interest at this time and obtain a clearer signal. Also, the Power Spectrum could give us some information about the conformational change itself and some of its properties. The PSD represents the energy per time unit that a signal carries in each part of the spectrum and is defined as follows for a signal with discrete time values [10]:

$$S(\omega) = \frac{(\Delta t)^2}{T} \left| \sum_{n=1}^{N} x_n e^{-i\omega n \Delta t} \right|^2 \tag{26}$$

This means the PSD is the square of the Fourier Transform of a signal. The result is usually shown in a loglog-plot. We must be careful when generating the PSDs for the trapping signals. If information about the nature of the trap is desired, we should only calculate the PSD of the trapping part of the signal. Including some of the signal where the laser has been turned off has significant impact on the resulting PSD. This happens because there are still data points being registered when the laser is off, with y-value close to 0. The jump (or jumps) in the signal will have a large impact on all of the frequencies in the PSD. This is illustrated in figure 20. The PSD in which the time without signal has been included, resembles the PSD of a square wave quite closely, as can be seen in figure 21. This makes it very hard to get any information about the actual trace from the PSD.

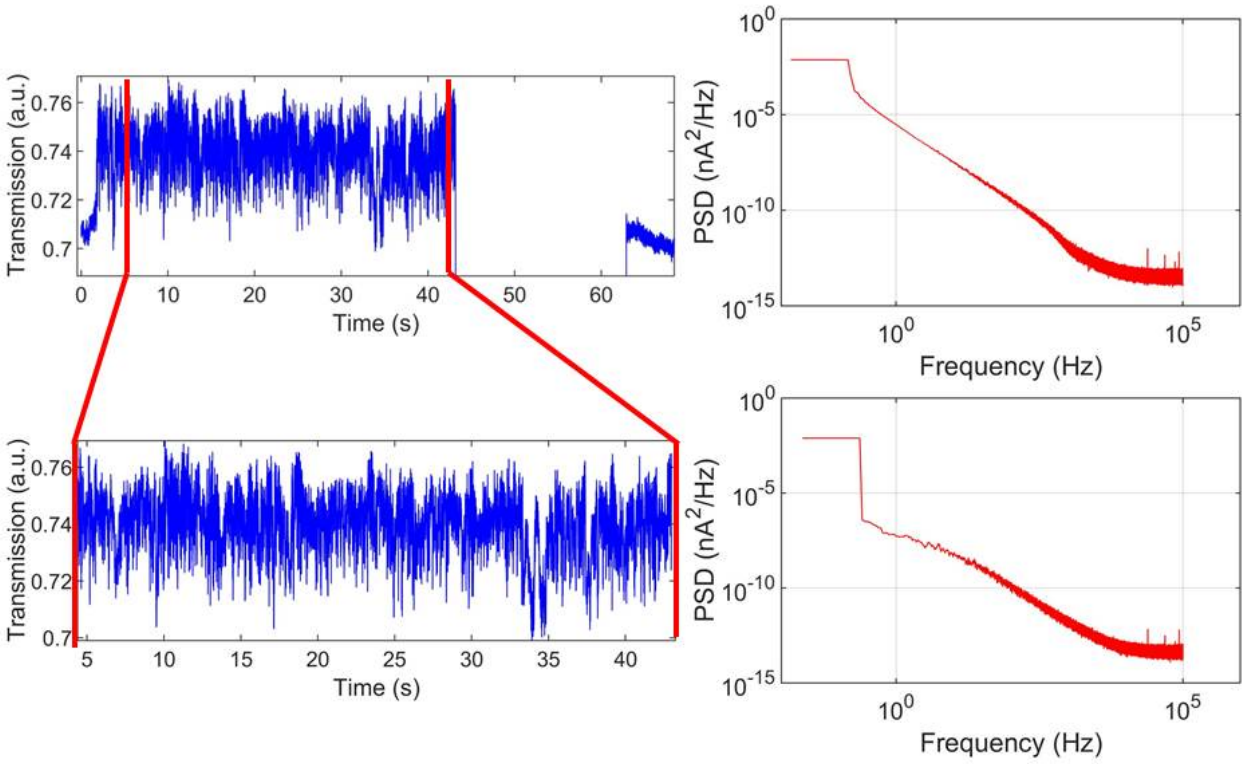

Figure 20: An illustration of the difference between PSDs generated from the signal with and without the signal generated when the laser is off. We see that the PSD which includes it contains barely any information about the trapping signal. It consists mostly of the $1/f^2$ ramp which is characteristic for a square wave.

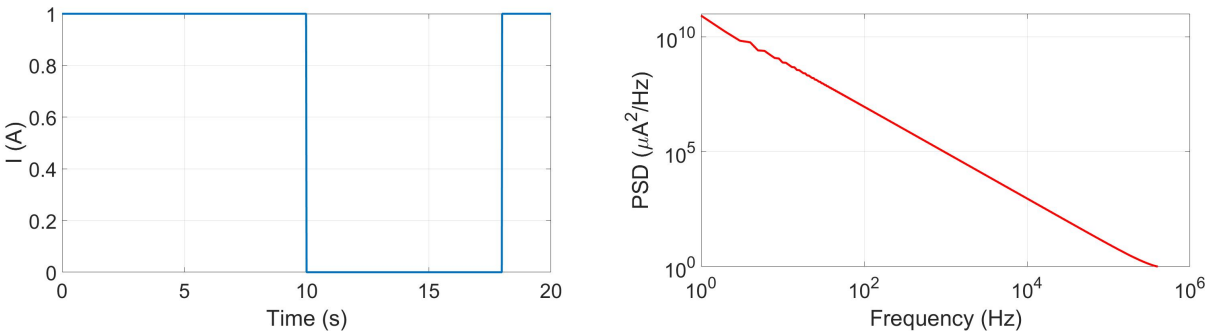

(a) Square Wave

(b) Associated PSD

Figure 21: The signal of an arbitrary square wave signal with 2 large jumps. Its PSD is shown in (b) in a loglog plot, where we see that it shows a line that decays with $1/f^2$. We now see that it resembles the PSD from figure 20 on the top right. Note: we know from theory that a square wave shows a $1/f$ pattern in Fourier space for its odd harmonics, and 0 for the even harmonics, but plotting zeros is not possible in a loglog plot. We therefore take the walking average over two data points, to obtain the plot shown, which tells us that the spectrum density decays with $1/f^2$.

3.6 Summary of Experimental Methods

The experimental setup consists of a laser and several optical parts for collimating, guiding and polarising the beam, after which it reaches the objective lense and the sample, containing the bow tie structures and the protein solution. The signal is finally recorded by the APD. The structures are fabricated using the process of focused ion beam milling of a silicon nitride membrane on a silicon chip, coated with gold. When scanning the surface with the laser, we see transmission of the bow ties when the laser is polarised in the resonance direction, but barely any transmission when we use the perpendicular polarisation. Polystyrene beads with a 20nm diameter will be used to compare the HSP90 results to. The signal will be corrected for drift and we will look at histograms that are created by dividing the y-axis into bins, after which the occurrences for each bin will be counted. The signal will be low-pass filtered to remove noise and to make the signal in the low-frequency part more visible, because that is where the conformational changes will show up. The power spectrum density is another way in which the traces will be analysed. With this technique, we visualise how much energy a signal contains in each part of the frequency spectrum. We proceed to perform trapping of HSP90 proteins in the subsequent section.

4 Results

In this section, we will first demonstrate the fact that we can trap HSP90 proteins for upwards of 30 seconds. After this, we will compare the trapping signal to the trapping signal of polystyrene beads, followed by a comparison between trapping HSP90 alone and trapping HSP90 with AMP-PNP. We will compare fluctuations in the trapping signals and the power spectra of the traces.

4.1 Stable trapping of HSP90 proteins for upwards of 30 seconds

As described in section 2.1, the HSP90 protein undergoes a conformational change every few seconds. Therefore, in order to be able to draw any conclusions about this change from the recorded traces, we must first make sure it is possible to trap the proteins for at least a few seconds on end in order to allow the protein to undergo several cycles of these changes. We pipette 0.2mM of HSP90 protein in 1X PBS (phosphate-buffered saline) solution into our inverted bowtie antennas. Upon addition of the proteins, we observe changes in the transmission of the inverted bow tie. Figure 22 shows the result of trapping HSP90 in the bow tie structures in a 0.2mM HSP90 solution. The figure shows that the HSP90 can be trapped very stably for upwards of 40 seconds, both in case of increasing and decreasing transmission during a trapping event, as described in figure 6.

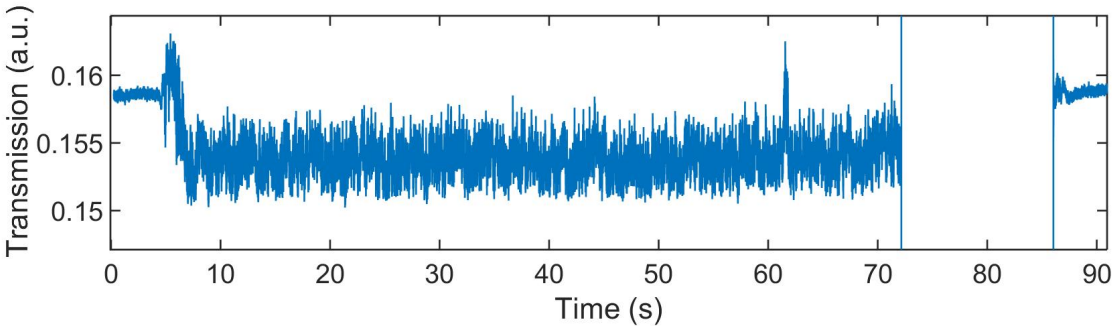

(a)

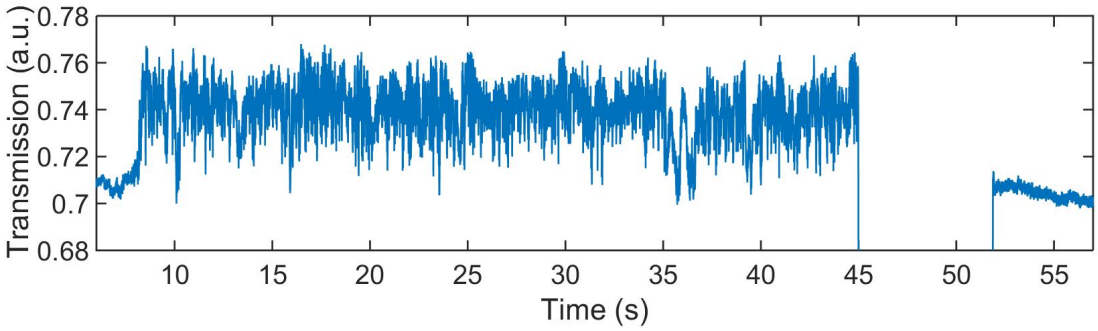

(b)

Figure 22: Two different HSP90 trapping events from 0.2mM HSP90 protein in 1xPBS solution. Both figures start at the baseline and continue to trap a protein. At some point both lasers are turned off and the proteins are free to escape. After a few seconds, the lasers are turned back on and the signals return to baseline. In (a) we see that the protein still has not left the trap after 80 seconds. The signal only returns to baseline after the laser has been turned off. The transmission during the trap is lower than the baseline, since the resonance wavelength of this bow tie is longer than the laser wavelength. The trapped protein redshifts this a little further away from the laser wavelength, resulting in lower transmission. Subfigure (b) shows the case where we are trapping on a bow tie with a shorter resonance wavelength than the laser, resulting in an increase in transmission during the trapping event. Just as in figure (a), the trap is stable enough to last over half a minute. After this time, a decision was made to turn off the laser and let it return to baseline to show that this was indeed a trapping event.

4.2 Increase in Transmission of HSP90

At this point, we would like to make a note that for the rest of the thesis, only bow ties with increase in transmission signal (resonance blue shifted from the laser wavelength) will be used. The reason is twofold.

First, many sources affect the baseline during the experiments. Most of these disturbances occur in three ways. The first possibility is a source of interference, causing sinusoidal noise in the signal, caused by mechanical vibrations, changes in air flow or activities in nearby labs. These are kept at a minimum by keeping the room at a relatively high temperature, so that the air conditioning doesn't interfere too much with the system, and by shielding the system with metal and cardboard covers to reduce the airflow.

The second form is noise. The setup has a bit of internal noise, arising mostly from thermal noise or small variances in the laser intensity. This effect is significantly reduced by turning on the laser well in advance of the experiments, on the scale of a few hours, so that the laser output can stabilise before the experiments are run.

The third type is a downward shift in intensity. This can be caused by a slight but sudden misalignment of the laser, any of the optical parts, something in solution flowing past, the sample drifting slightly or clogging of the aperture. All of these will cause the signal to shift downward. We try to work with traces that have an increased trapping signal as much as possible, in order to prevent mistaking such a disturbance for a trap. Granted, the signal would never return to baseline after such a disturbance, but that would only be discovered afterwards.

The second reason for choosing these traces results from the way the trapping works. Both signal types may result in a stable trap, but there still is a fundamental difference in the way the traps work. If we look back at the way the trapping phenomenon emerges from the electric field gradient force, we can see this difference arise.

A trapping signal with higher transmission means that the presence of the bead or protein increases the electric field, and therefore also the strength of the trap. On the other hand, a lower trapping transmission results in a trap that becomes looser upon the entrance of a bead or protein. Both types of trapping create a different shape of potential well, which could cause significant differences in the signal and the power spectrum.

We want to investigate the conformational changes in HSP90 and our strategy includes comparing the signal of trapped HSP90 to trapped beads. In order to draw credible conclusions from the comparison, we need to make sure that most other circumstances are kept constant throughout the experiments, since any change in circumstances could cause a change in the signal. For this reason it is important to be consistent in our choice. Therefore, it is decided to stick with the signals with increasing transmission throughout this research.

4.3 Comparison between Signals from HSP90 and from Beads

The possibility to trap a single protein for such a long time makes this method useful for investigating the nature of the conformational change. We hypothesize that the conformational states cause different transmissions and will show up as different levels in the signal. In order to test this hypothesis, we will compare the trapping signals of our HSP90 trap to the signal of the trapped polystyrene (PS) beads. Of these beads we can be sure that they do not show a conformational change, so some of the differences that emerge in the trapping signals can lead us to more understanding of the conformational change.

To tease out the differences, we added 0.05% concentration of 20nm PS beads, which are not expected to show a conformational change, in 1x PBS solution into the sample. We then measured the signal. Figure 23 shows the result obtained from one of the bow ties with an increase in transmission. We see a sharp increase, after which the trapping signal seems noisy. The trace for the PS beads seems to have a very constant maximum transmission, where the HSP90 trace does not. For both traces, the noise seems to have a high frequency, or at least much higher than the $\sim$1 Hz that the conformational change should show, so it is decided to apply a low-pass filter to both signals. The result of the 10Hz low-pass filter for both signals has been enlarged in figure 24.

Figure 23 shows a comparison of both signals, both the original signals and after low-pass filtering with 100Hz and 10Hz. In the figure, we can see that the bead trapping signal reduces to almost a flat line. This creates a very sharp peak in the histogram, whereas the peak in the HSP90 histogram is not reduced to the same sharpness, and only slightly separates from the baseline peak.

This difference that arises when filtering the signals could have a few different causes. In the methods section about signal correction, we have shown that a slight drift in the signal can lead to very chaotic behaviour in the histogram. It could therefore be the case that we are looking at a signal that is subject to a drift. We have a little bit of evidence for this, as the HSP90 baseline after the trap is not very stable. If this were the only reason, however, we would expect the signal itself to look almost like a straight line, albeit with a little drift. This is clearly not the case, as we can tell again from the enlarged comparison in figure 24.

In figure 24, we can see that the HSP90 trapping signal is still very chaotic after low-pass filtering with 10Hz, whereas the filtered bead trace has become almost a straight line. We also see that this difference is not caused by a difference in zoom between the two figures, because both signals see an increase of 5%-6% in the trapping signal relative to the baseline. There should therefore be an actual difference between the two trapping events, so we will investigate other possible causes.

One possible cause for the more chaotic signal could be interference from outside the sample. This includes anything that results from mechanical vibrations or from air flows or vibrations outside the experimental setup. It is difficult to check such a large number of possibilities, but we do know that it must be something lower than 10Hz, because it would have been filtered out otherwise. We can easily search for such vibrations by inspecting the power spectrum densities (PSDs) of both signals. Figure 25 shows the result. A comparison of signals and their respective PSDs shows that the HSP90 trace used before is not perturbed by sinusoidal interference, since 25(c) shows what that would look like: a clear bump in the power spectrum around the 5 - 10Hz spectrum. We conclude that the distribution in the HSP90 signal as shown in figure 23(f) is not caused by sinusoidal interference from outside the setup.

In the trace analysed in this example, we do not see a lot of drift in the signal, but we do see that in one of the traces in the supplementary information. This drift makes it very difficult to analyse the signals using the techniques used here. We could look at band-pass filters that filter out some very low frequency drift in the signals, but then we would also risk filtering away some of the signal from the conformational change.

Taken together, we conclude that the 'chaotic' signal from the HSP90 trace is indeed due to the dynamics of the protein since other sources are not plausible. Most strongly, the protein signal does not reduce to a 'step' signal similar to the PS bead trace when filtered at 10Hz.

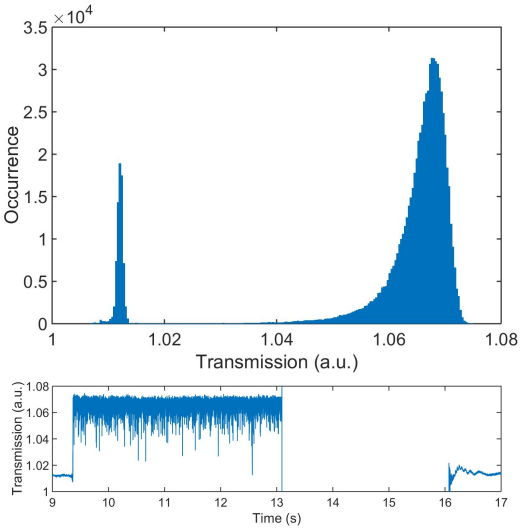

(a) Bead - Original Signal

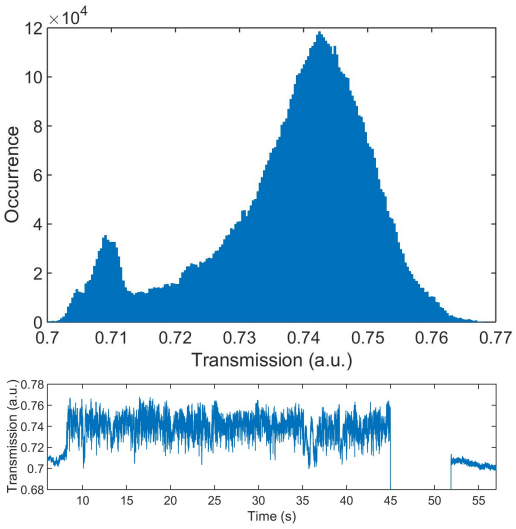

(b) HSP90 - Original Signal

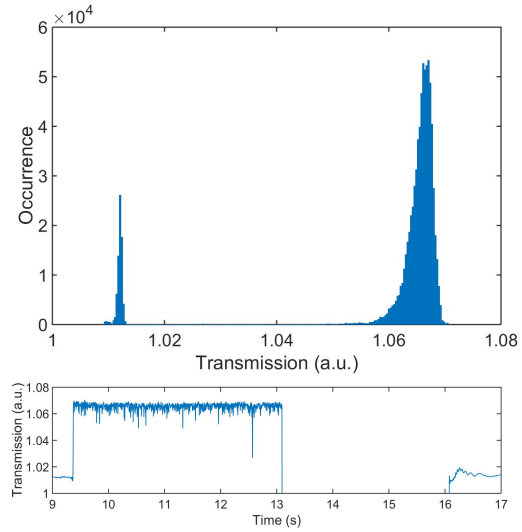

(c) Bead - 100Hz Low Pass

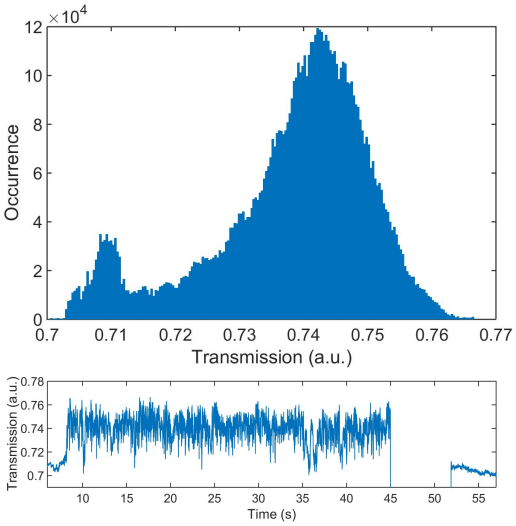

(d) HSP90 - 100Hz Low Pass

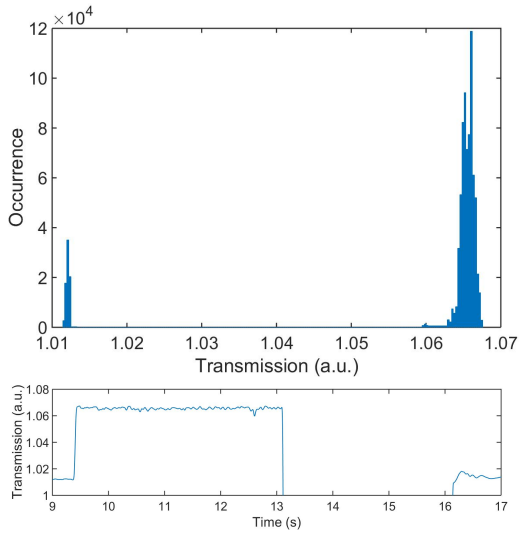

(e) Bead - 10Hz Low Pass

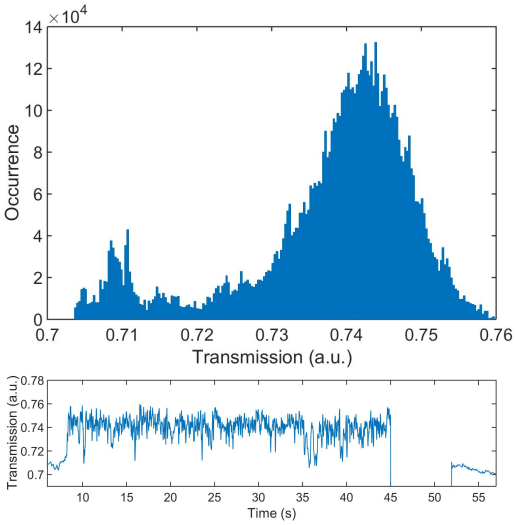

(f) HSP90 - 10Hz Low Pass

Figure 23: A comparison of the HSP90 trapping signal with the bead trapping signal. We see that the bead trap has a very constant maximum with downward noise spikes, while the HSP90 trace seems to extend both upwards and downwards. Where filtering reduces the bead trapping signal to a nearly straight line, this doesn't happen with the HSP90 signal. This becomes clear from the trapping signal itself, but even more from the distribution in the histograms. The signals from subfigures (e) and (f) have been enlarged and can be compared in figure 24.

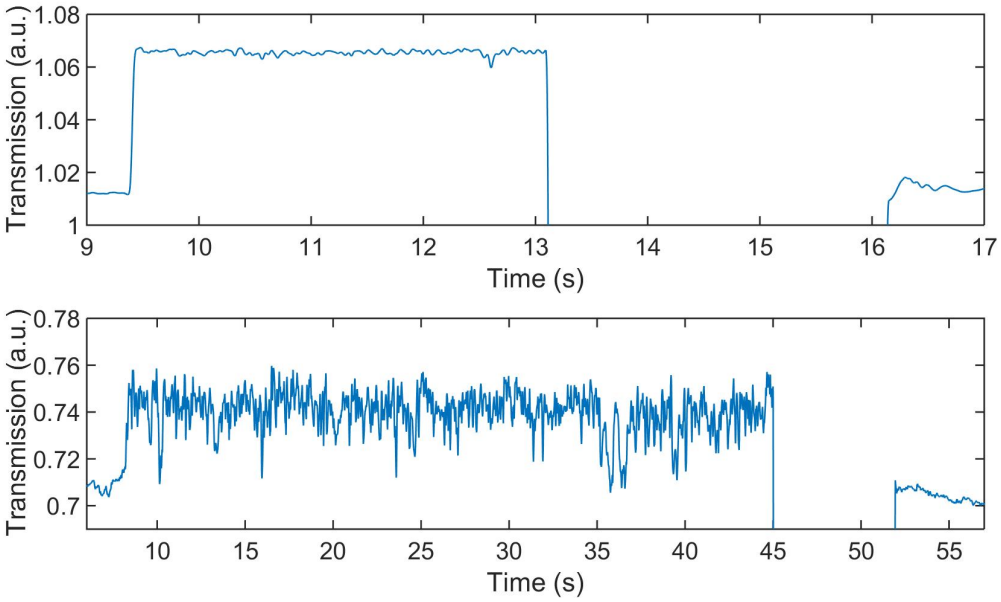

Figure 24: Comparison of 10Hz low-pass filtered signals from beads (top) and HSP90 (bottom). We see that despite the same filter and same baseline increase of $\sim$ 5-6%, the HSP90 undergoes a lot more chaotic transmission increases compared to the 20nm PS beads.

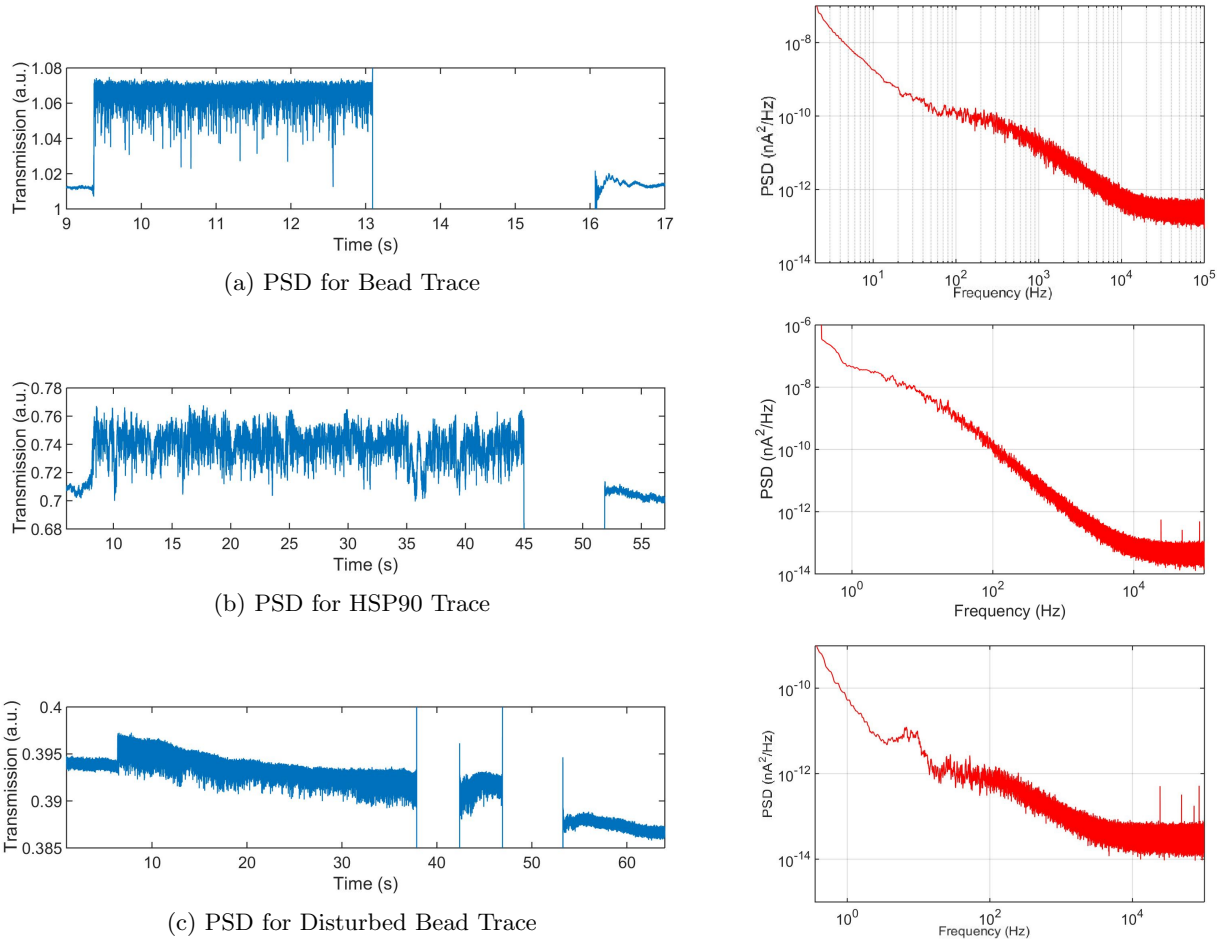

(a) PSD for Bead Trace

(b) PSD for HSP90 Trace

(c) PSD for Disturbed Bead Trace

Figure 25: A comparison of three trapping traces with their respective PSDs. Subfigure (a) shows the bead trace with its PSD next to it, subfigure (b) shows the same for the HSP90 trace used before and subfigure (c) shows a bead trap while there was acoustic noise in the 5Hz - 10Hz part of the spectrum, which also shows up as a bump in the PSD. This shows that the distribution of the HSP90 signal cannot be explained by the same source of noise.

4.4 Possible explanations for the lack of 2 levels

Finally, another possibility is that we are looking at a phenomenon caused by the conformational change in the HSP90. If this is the case, then it does not appear exactly in the way that we had expected it to. According to the expectation, there should have been two clearly distinguishable levels visible in the distribution, but that is not the case. We will have to carry out more experiments in order to determine if the distribution is caused by the conformational change.

Changing very quickly between the levels could be the cause for not being able to distinguish the levels. This would mean that the HSP90 spends a significant amount of time transitioning from one state to the other, all of which ends up in the final histogram. Low pass filtering helps filtering out noise, but it would certainly not help with fixing this problem. In fact, it would only make the problem worse, since filtering the high frequencies smooths the signal.

4.5 Analysing the effect of AMP-PNP on HSP90

HSP90 cycles through the two conformational states binding ATP, hydrolysing it and releasing the formed ADP [6]. The relation between the ATPase rate and the rate of confomational change is still under investigation [9], but we can still use this to inhibit the conformational change [5]. The N-terminus of HSP90 contains an ATP-binding site, which can be inhibited by AMP-PNP (Adenylyl-imidodiphosphate), a structural analogue of ATP, though non-hydrolysable [22].

AMP-PNP inhibits this function of HSP90, so it is expected to decrease the probability of changing conformation to some degree. We foresee several possible outcomes. One possibility is that the AMP-PNP completely locks the HSP90 into either one of the two states. Another would be that the AMP-PNP somewhat slows down one or both transitions, leading to stronger separation of the expected two levels. The latter is what we expect, looking at the results from [15].

In order to see what happens, we pipette a solution with 0.5mM HSP90 and 2mM AMP-PNP in 1x PBS solution into the sample. With these concentrations, the chance to find an HSP90 protein coupled to an AMP-PNP molecule, should be very high. Figure 26 shows the trap that results. The protein does not directly leave the trap after turning off the laser for the first time, but it does eventually leave after the laser has been left off for slightly longer.

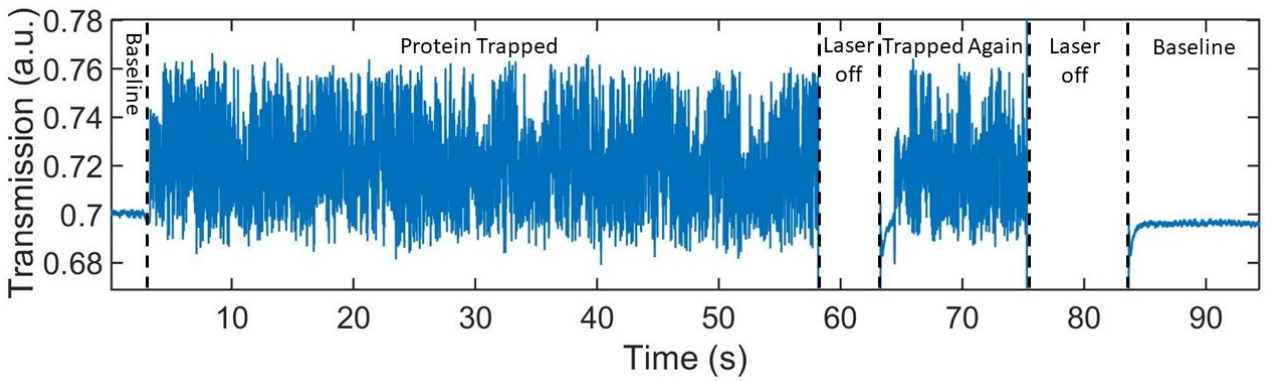

Figure 26: An event measured in a bow tie with increasing transmission in a solution of 0.5mM HSP90 with 2mM AMP-PNP in 1x PBS solution. We see that the protein gets trapped in the bow tie and the signal increases. When the trap lasts more than 50 seconds, the laser is turned off. When the laser is turned back on again, the protein gets trapped again. This probably happens because the protein has not drifted far enough away from the bow tie in the time given. When the laser is turned off for slightly longer, and then turned back on, the protein has left the trap and the signal returns to baseline.

We see that the signal shows noise that is more like the HSP90 trace from before than like the bead trace. It is not really possible to draw any conclusions from the signal by eye. Therefore, we use the technique from before and apply low-pass filters to the signal. For each signal, we also create a histogram as we have done before.

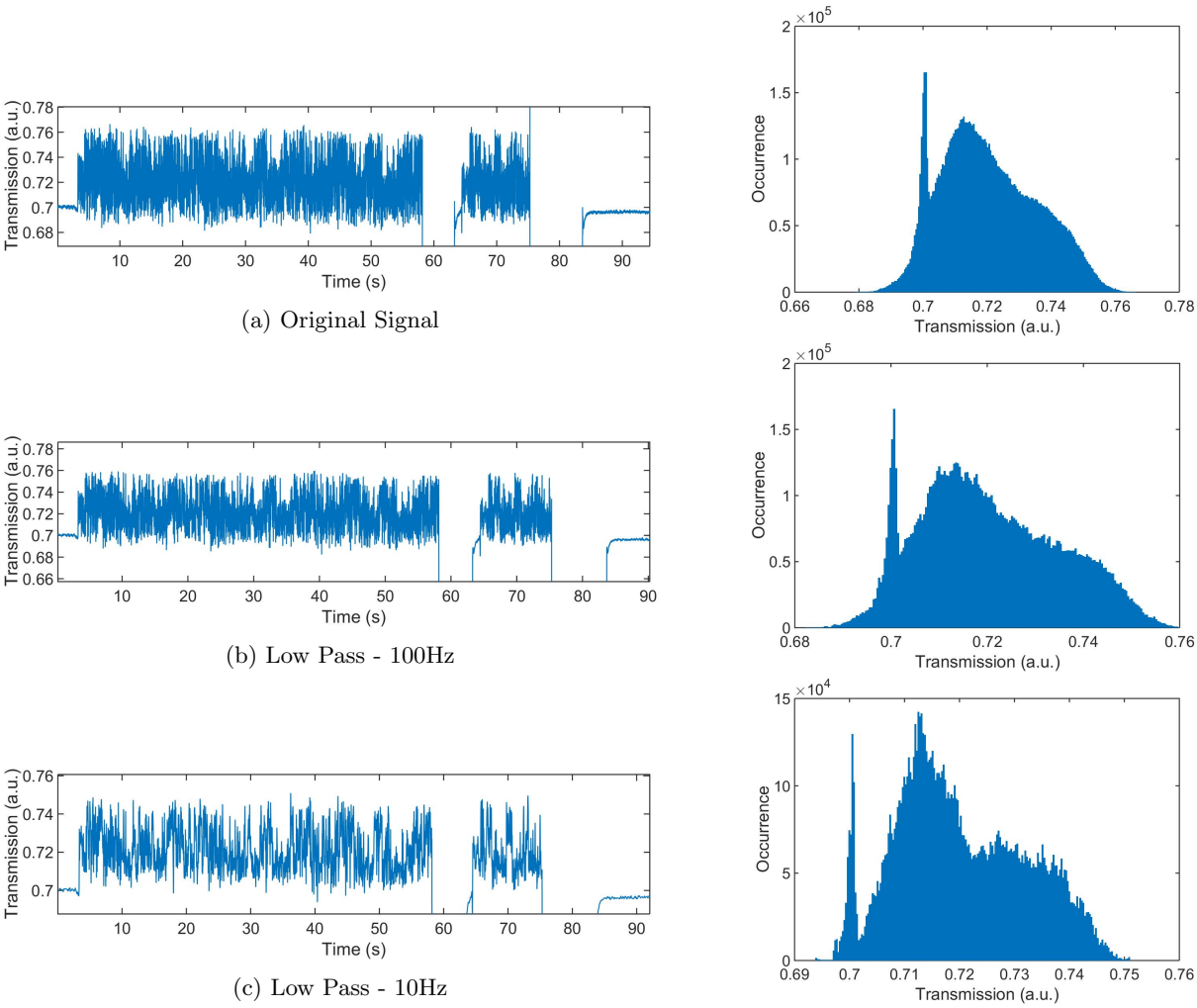

(a) Original Signal

(b) Low Pass - 100Hz

(c) Low Pass - 10Hz

Figure 27: Trapping signal of HSP90 with AMP-PNP. Subfigure (a) shows the original signal including the histogram of y-values. Subfigures (b) and (c) show the result after low-pass filtering the signal. In each plot, we clearly see the baseline appearing as a sharp peak around 0.7. In (a), we already notice that the distribution of the trapping signal is very different from the signals we have seen before. Subfigures (b) and (c) confirm this, because we see that the distribution consists of two peaks. The peaks that result have not been separated completely yet. We also note that the protein does not leave the trap on the first time that the laser is turned off and on. The first time it returns into the trap quickly after the laser has been turned on, probably because it was still near the trap and it had not had enough time to escape far enough. The second time we turn the laser off and on, the protein does not return after the laser has remained off for a slightly longer time. In this way we show that the protein was not stuck inside the bow tie, but was actually trapped.

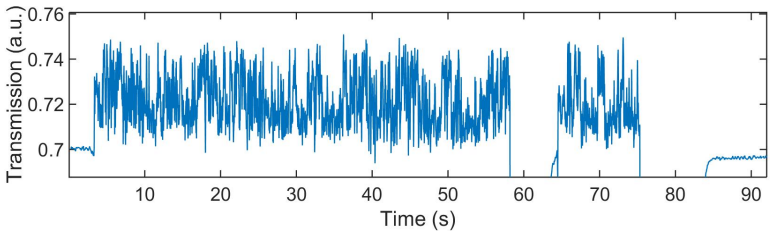

Figure 28: Enlarged trapping signal of HSP90 with AMP-PNP after a low-pass filter with cutoff frequency at 10Hz. If this turns out to be a two level system, then it is not immediately clear which part of the signal belongs to which level on visual inspection.

Figure 27 shows the result of trapping HSP90 with AMP-PNP. A baseline peak is clearly visible in all the histograms and it separates from the rest of the distribution after filtering. The rest of the distribution seems to resemble a two level system, but the two levels do not separate after filtering, even at 10Hz. The fact that the distribution does fit nicely to two normal curves is illustrated in figure 29.

After dividing the range into bins of $5 \cdot 10^{-4}$mV and creating a histogram, it becomes clear that the distribution fits very well to the distribution of two normal curves (R-square = 0.9988), as we expected after looking at the filtered signals from the trapped HSP90 with AMP-PNP. However, even after low-pass filtering at 10Hz, the two peaks do not yet completely separate from each other. This results in the fact that it is not possible to determine which parts of the trace belong to which level, because there is quite a large domain where a significant portion of both levels will end up. This also becomes clear in figure 28, which shows an enlarged version of the trapping trace, after a low-pass filter with cutoff at 10Hz has been applied.

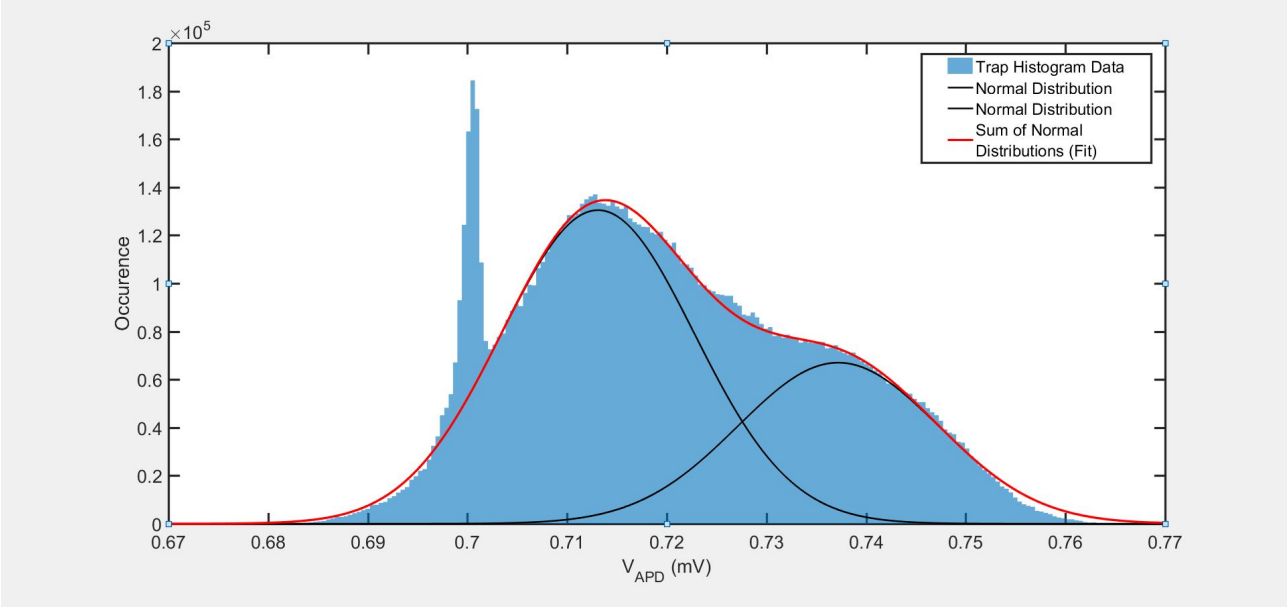

Figure 29: Histogram of HSP90 with AMP-PNP trapping signal, counted in bins with size $5 \cdot 10^{-4}$mV. A fit has been made to the distribution with two added normal distributions. The red line represents the total fit and the black lines represent the normal distributions that it consists of. We see that the distribution very closely fits the addition of the two normal curves. The base line peak has not been taken into account when fitting. The distribution was fit to the function $y = Ae^{-c(x-f)^2} + Be^{-d(x-g)^2}$, resulting in the values (with 95% confidence bound) $A = (1.474 \pm 0.033) \cdot 10^5$, $B = (2.87 \pm 0.04) \cdot 10^5$, $c = 4937 \pm 384$, $d = 5349 \pm 230$, $f = 0.7372 \pm 0.0005$, $g = 0.7131 \pm 0.0002$. The R-square for this fit is 0.9988.

4.6 Interpretation of the double normal distribution

Then the question remains what we are actually looking at here. The two level system is quite convincing, but we have no indication of what it represents. We will give a few possible explanations for the resulting two level system. A first possibility is that this specific bow tie creates two spatially separated potential wells. Each potential well is then represented by one of the two states. They both have a different effect on the transmission, causing the two peaks to appear on different levels. The difference in height of the peaks would then be explained by the fact that one of the wells is a little deeper and the probability of the protein residing there is higher. This explanation is not very likely, as the small differences in the dimensions of the bow ties will not result in such large changes in the potential well.

Another possibility is that we are looking at something that has to do with the shape of HSP90. The beads that we have looked at before are nearly spherical, but the HSP90 is not. The electric field gradient force pulls on every piece of volume with equal strength, so assuming a constant density, that means it would not induce a rotation to force the protein in a certain orientation. It is possible that the changes in signal strength in the HSP90 signal in figure 24 are caused by the rotation of the protein. The rotation could cause some deviation in the transmission, where the average is determined by the conformational state that the protein is in. If the AMP-PNP inhibits the conformational change to one side more than to the other side, that would explain the resulting histogram shown in figure 29.

It is possible to run experiments to either prove or to rule out the possible explanations for the results. The hypothesis that there are multiple minima in the potential well can be tested by trapping in differently shaped structures. In order to do this, we should find variation in all three dimensions, because a priori, we cannot be sure what the positions of the minima are relative to each other. This could also be tested by running more finite difference time domain simulations of altered shapes in 3D. The rotation hypothesis could be proven experimentally by comparing trapping events from proteins that are almost spherically symmetric with proteins that are shaped more like a rod or like a disk.

4.7 Spectral Analysis

Another way of investigating the difference between the traces is by inspecting the Power Spectrum Densities (PSDs). The PSD of a trace is defined as the square of the magnitude of the fourier transform. This is a measure for the amount of energy (or power) the signal has in a certain domain of the spectrum. The actual analysis of the PSDs generated from a trapping signal with HSP90 will be covered in section 4.7.2. Before we get to that, we will first explore what we would expect the conformational change to look like in a PSD plot. This will be covered in the next part.

4.7.1 Model for Telegraph Noise

If the conformational change shows up as two levels that are slightly separated, as was suggested by the experiments with HSP90 in combination with AMP-PNP in section 4.5, then the signal can be modelled by what is called telegraph noise, or burst noise [13]. This type of noise can take two values, and at every moment, it has a certain probability of jumping to the other level.

We can model this in MATLAB and calculate the PSD of such a signal. The result of generating such a signal is shown along with its PSD in figure 30. This has been generated with $p_1 = 2p_2$, where p_1 is the probability of jumping up when the signal is low, and p_2 is the probability of jumping down when the signal is high. It turns out that changing the ratio of probabilities does not change the shape of the PSD.

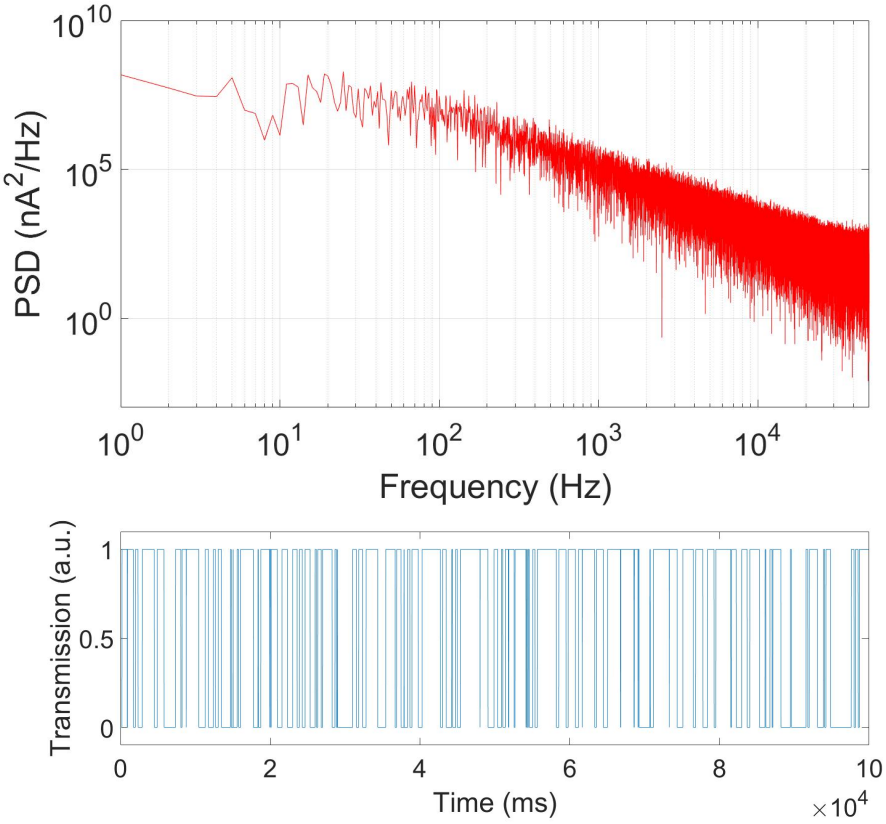

Figure 30: Generated telegraph noise signal with its PSD. We see that the spectrum consists of two parts. In the low frequency range, it has a constant density. In the higher frequency range, it drops off with $1/f^2$.

The PSD belonging to the telegraph noise always has roughly the same shape. In the low frequencies, it is constant, but at some point it starts to decay with $1/f^2$. If the conformational change shows up in the PSDs from HSP90 traps, we expect the resulting PSD to look like an addition of the telegraph PSD and a PSD generated by trapping something without a conformational change. This can only happen if the conformational changes appear as two levels in the trapping signal, and if the change takes place as a memoryless process, and this last condition is something we expect. We will now continue by taking a look at the power spectra that result from trapping signals.

4.7.2 Power Spectrum of HSP90 Traces

Figure 31 shows the typical power spectrum of a HSP90 trapping signal.

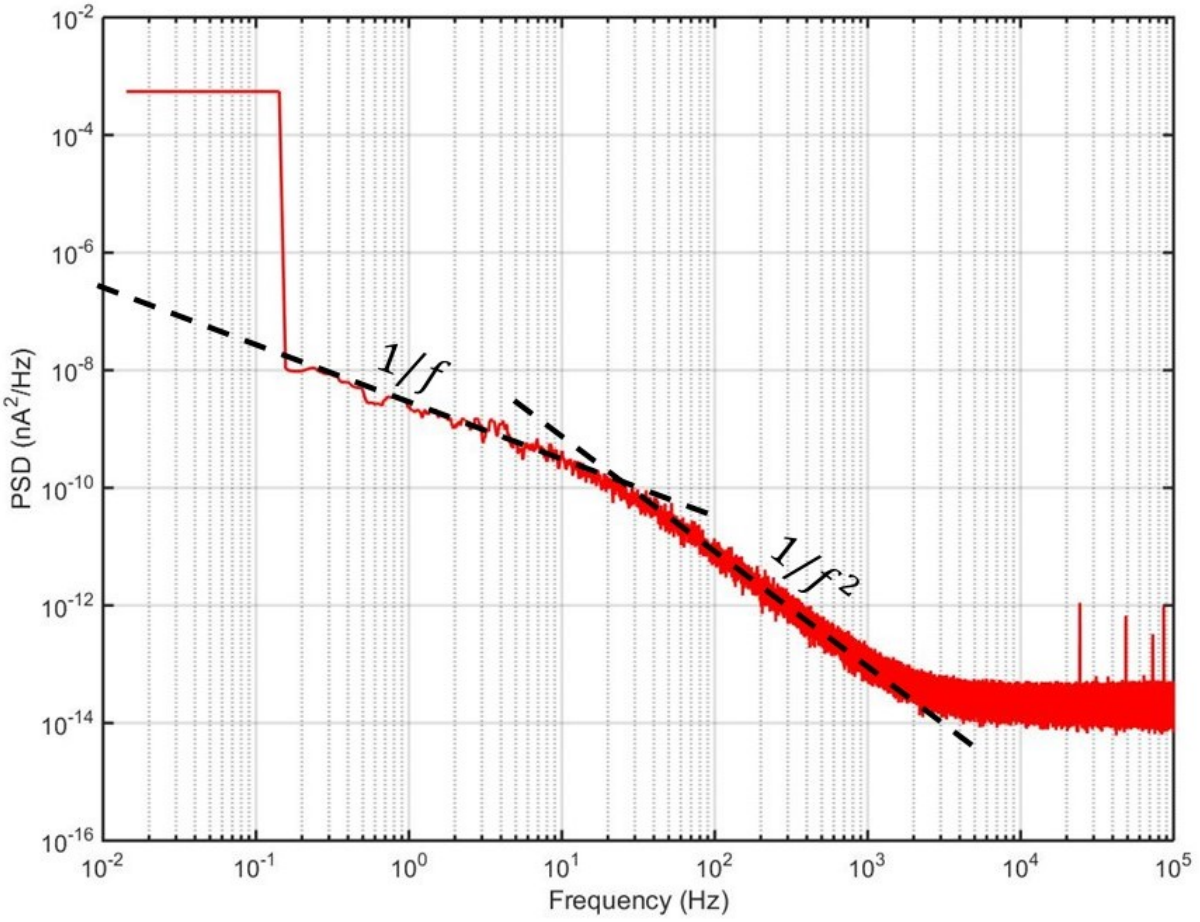

Figure 31: Power spectrum density of the HSP90 trapping signal. The spectrum seems to consist of three parts. The first part is proportional to $1/f$, the second part is proportional to $1/f^2$ and the last part is white noise, which is constant over the entire frequency spectrum.

The typical PSD for a trapping trace has multiple sections. In the lower frequency domain, it decays with $1/f$, thereafter with $1/f^2$ and the final part consists of white noise. There are many possible sources for these types of noise, of which Edoardo Milotti has reviewed a good number [11]. Especially the explanation based on a superposition of relaxation processes seems to fit the situation at hand. The power spectrum as a consequence of such a phenomenon would be as follows:

$$S(\omega) = \begin{cases} C, & \text{for } 0 < \omega \ll \lambda_1 \ll \lambda_2 \\ \frac{C\pi}{2\omega(\lambda_2 - \lambda_1)}, & \text{for } \lambda_1 \ll \omega \ll \lambda_2 \\ \frac{C}{\omega^2}, & \text{for } \lambda_1 \ll \lambda_2 \ll \omega \end{cases} \tag{27}$$

Where C is an arbitrary constant. This seems to describe the observed PSD quite well. In fact, if we can prove that this power spectrum shape is linked to the conformational change, then the λ_1 and λ_2 might be constants that describe the rate of the conformational change in the HSP90 proteins. To check this, we compare the PSDs of the different traces side-by-side in figure 32.

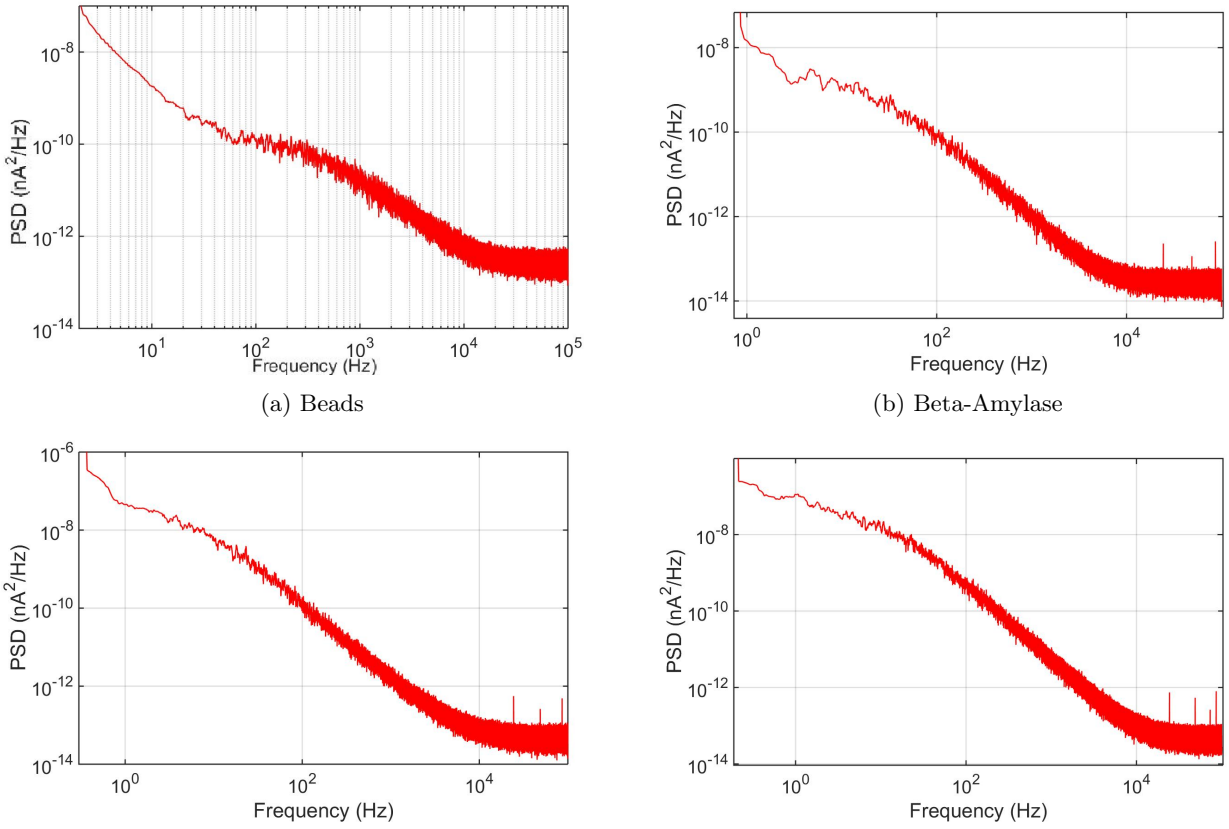

(a) Beads

(b) Beta-Amylase

(c) HSP90

(d) HSP90 w/ AMP-PNP

Figure 32: PSDs of the three traces used in previous sections: the bead trace, a beta-amylase trace [19], the HSP90 trace and the HSP90 with AMP-PNP trace. All three traces show roughly the same shape, only the bead trace is a bit different in the low frequency spectrum, but this is caused by the shorter length of the trace. The bead trace is a little too short to result in a clear PSD. A beta-amylase trapping PSD has been added as a substitute to compare the HSP90 PSDs with.

Since the bead trace was a little too short to give us information about the low frequency part of the spectrum, we chose to compare the HSP90 traces to a Beta-Amylase trace. Beta-Amylase is a protein with a much less complicated structure than HSP90 [14]. It should not show the same conformational change. For this reason, we use its PSD to compare the HSP90 PSD with.

All of the PSDs from trapped particles have a large part of the spectrum that is proportional to $1/f^2$. This is unfortunate, since we expected the conformational change to show up with roughly the same profile. It is therefore pretty unlikely that we will be able to extract information about the conformational change from the PSDs. We can also say that with the PSDs we have at our disposal at this moment, we cannot say for certain that the conformational change is showing up in the trapping signal as we had hypothesized.

Since the properties of all PSDs are so similar, we conclude that the PSD shapes are not mainly caused by the behaviour of the proteins, but for the most part by the characteristics of the trap. The parameters λ_1 and λ_2 can probably not tell us much about the rate of the conformational change.

4.8 Summary of Results

The first experiments were run with the goal of showing whether or not HSP90 proteins could be trapped stably. We quickly saw that this was indeed possible for upwards of 30 seconds. In fact, the traps would probably be stable for longer periods, because the protein only left the trap when the laser had been turned off. See the appendix for a trace where we trapped HSP90 for 3 minutes. We chose to proceed to the rest of the results with traps that showed an increase in transmission when a protein was trapped, for practical reasons (noise, stability) and for consistency.

Next, we compared the traces from HSP90 trapping events with those from beads and looked at the respective histograms. We also compared these traces and the histograms after applying 10Hz and 100Hz low-pass filters to the signals. From this, it became very clear that there were some large differences between the HSP90 and the beads under trapping conditions. Namely, the HSP90 signal is a lot more chaotic when looking at the trapping signal. After applying a 10Hz low pass filter, we see that it is clearly more chaotic in the low frequency spectrum, even though both traces show the same relative transmission increase of around 5%. We also note that it does not clearly show a 2 level system in the histogram.

To investigate whether this difference was caused by the conformational change, we discussed some other possible causes, such as noise or sinusoidal interference, and disproved them. We ran experiments to trap HSP90 proteins with AMP-PNP, the structural ATP analogue which is known to slow down the conformational change. When trapping this complex, we did see strong evidence for a two level system. The histogram fit very well ($R^2 = 0.9988$) to the addition of two normal distributions, but the two peaks did not separate after applying a 10Hz low pass filter. At this resolution, it is impossible to conclude that the two peaks in the histogram were indeed due to the two conformational states in the protein.

In the last part, we investigated whether we could draw more conclusions from the power spectrum densities of the trapping events. We calculated what the power spectrum density would look like if the conformational change showed up as two levels in the final trace in the form of telegraph noise. It turned out that the spectrum of this process would not look very different from what most of the trace spectra look like. We therefore concluded that the conformational change would probably not show up in the power spectrum of a trace, even if it would appear as a two level system.

Taken together, these results suggest that optical trapping with assistance from plasmonic nanoapertures is a very good way of studying proteins without causing much disturbance to the proteins or their direct environment. More work needs to be done to ascertain whether we are seeing the conformational change in the HSP90 protein that we trapped. We will discuss this in the concluding chapter.

5 Conclusion

The goal of our experiments was to investigate whether we could study the conformational change in HSP90 protein by using plasmonic nanoapertures. In this part we will conclude whether that is the case based on the results obtained during the experiments in this thesis.

First, we created a heat flow model of our nanoapertures and showed that the temperature increase could be limited to a level where it would not disturb the proteins (20X reduction in the heat for the same laser trapping power). Using a 3D random walk model, we showed the behaviour of a protein in the trapping area.

We motivated the shape of the apertures that we would use. We verified that the fabricated inverted bowtie structures indeed showed the predicted resonances by scanning the bowtie array with two perpendicular polarisations. We only saw a strong increase in transmission for the polarisation direction that was parallel to the short side of the bow tie. We devised a stabilisation protocol in order to better stabilise the baseline for the experiments.

We demonstrated stable trapping and detection of proteins. We saw that the transmission did indeed show the predicted increase or decrease when a trapping event occurred. We verified that the protein was indeed optically trapped because the HSP90 protein did not leave the trap on its own during the first 30 seconds of the trapping event and only left the area when the laser had been turned off for a few seconds. We conclude that it is possible to obtain a stable trap for over 30 seconds with HSP90 protein. We chose to investigate the results from the traces with an increasing transmission, to decrease the risk of mistaking obstructions for a trap and because of consistency.

Next, we performed optical trapping of 20nm PS beads and compared the trapping signals from HSP90 proteins and beads. We hypothesised that the beads do not undergo a conformational change, and therefore would have differences in the trapping signals. We could see that the trapping signals did indeed look very different. In particular, the trapping traces from the HSP90 exhibit more fluctuation, higher low frequency noise and increases above the average trapped intensity levels unlike the beads trace which had a stable maximum intensity value. This point was even more remarkable when we applied a low pass filter at 10Hz. The bead trace reduced to a single 'step like' trace while the HSP90 showed a more 'chaotic' signal. We investigated other possible causes of differences in the trapping signal such as due to noise, drift of the baseline and interference from outside the setup and verified that this was not the case. Notably we did not see a clear 2 level system that was expected from the conformational change of the trapped protein even after extensive low pass filtering the signal to remove high frequency noise.

An experiment was run using a solution of HSP90 with AMP-PNP, which should slow down the conformational change. The resulting signal did seem to show two levels, although the peaks in the histogram were not completely separate. We saw, however, that the distribution of the trapping signal fit nearly perfectly so the sum of two normal distributions ($R^2 = 0.9988$). We tried to look for other methods to determine a difference in signal that we could attribute to conformational change. We tried looking at the shape of the power spectrum density of the trapping signal and modelled how such a system should look with a PSD of a telegraphic noise signal.

We conclude that there is some evidence that the conformational change causes a two level system in the trapping signal, although it does not show up as clearly as expected. We cannot determine very easily which part of the signal represents which of the two levels, since the peaks do not completely separate from each other. In order to do this, we propose that one could try using a method for signal analysis which is more complex than creating a histogram of the transmission values and also uses the time values of the data points, which the histogram does not, such as a Hidden Markov Model approach.

All in all, we conclude that trapping the HSP90 protein using plasmonic nanoapertures is a very good way of stably confining a single protein, without having to physically attach it to a surface and without generating too much heat. Also, it allows for direct detection in the transmission without the need of labelling the protein. This makes the method very suitable to study the conformational change, but we will need more powerful ways of analysing the signal to be able to draw conclusions about the parameters of the conformational change.

References

[1] A. Ashkin. Acceleration and trapping of particles by radiation pressure. *Physical Review Letters*, 1970.

[2] B. Chen, D. Zhong, and A. Monteiro. Comparative genomics and evolution of the hsp90 family of genes across all kingdoms of organisms. *BMC Genomics*, 2006.

[3] G. Crevel, H. Bates, H. Huikeshoven, and S. Cotterill. The drosophila dpit47 protein is a nuclear hsp90 co-chaperone that interacts with dna polymerase alpha. *Journal of Cell Science*, 2001.

[4] C. Garnier, I. Protasevich, R. Gilli, P. Tsvetkov, V. Lobachov, V. Peyrot, C. Briand, and A. Makarov. The two-state process of the heat shock protein 90 thermal denaturation: effect of calcium and magnesium. *Biochemical and Biophysical Research Communications*, 1998.

[5] M.P. Goetz, D.O. Toft, M.M. Ames, and C. Erlichman. The hsp90 chaperone complex as a novel target for cancer therapy. *Annals of Oncology*, 2003.

[6] N. Grammatikakis, A. Vultur, C. Ramana, A. Siganou, C. Schweinfest, D. Watson, and L. Raptis. The role of hsp90n, a new member of the hsp90 family, in signal transduction and neoplastic transformation. *Journal of Biological Chemistry*, 2002.

[7] L.P.B.M. Janssen and M.M.C.G. Warmoeskerken. *Transport Phenomena Data Companion (pages 102-111, 121)*. VSSD, 2006.

[8] R. Koebler. Optical trap/optical tweezer: explanation with focused laser. *https://commons.wikimedia.org/wiki/File:Optical_trap_focused.svg*, 2011.

[9] M. Mickler, M. Hessling, C. Ratzke, J Buchner, and Th. Hugel. The large conformational changes of hsp90 are only weakly coupled to atp hydrolysis. *Nature Structural & Molecular Biology*, 2009.

[10] S. Millers and D. Childers. Probability and random processes. *Academic Press*, 2012.

[11] E. Milotti. 1/f noise: a pedagogical review. *arXiv Physics*, 2002.

[12] Y. Miyata, H. Nakamoto, and L. Neckers. The therapeutic target hsp90 and cancer hallmarks. *Current Pharmaceutical Design*, 2013.

[13] B. Rajendran. Random telegraph signal (review of noise in semiconductor devices and modeling of noise in surround). -, 2006.

[14] Martin Rejzek, Clare E. Stevenson, Andrew M. Southard, Duncan Stanley, Kay Denyer, Alison M. Smith, Mike J. Naldrett, David M. Lawsona, and Robert A. Field. Chemical genetics and cereal starch metabolism: structural basis of the non-covalent and covalent inhibition of barley beta-amylase. *Molecular BioSystems*, 2010.

[15] S. Schmid, M. Götz, and T. Hugel. Single-molecule analysis beyond dwell times: Demonstration and assessment in and out of equilibrium. *BioPhysical Journal, Vol. 111, Issue 7*, 2016.

[16] A.K. Shiau, S.F. Harris, D.R. Southworth, and D.A. Agard. Structural analysis of e. coli hsp90 reveals dramatic nucleotide-dependent conformational rearrangements. *Cell*, 2006.

[17] D.R. Southworth and D.A. Agard. Client-loading conformation of the hsp90 molecular chaperone revealed in the cryo-em structure of the human hsp90:hop complex. *Molecular Cell*, 2011.

[18] T.M. Squires and S. R. Quake. Microfluidics: Fluid physics at the nanoliter scale. *Reviews of Modern Physics*, 2005.

[19] M.C. Van Dijk. Optical nanotweezing of beta-amylase proteins with plasmonic nanoapertures. *TU Delft Education Repository*, 2018.

[20] D Verschueren, X. Shi, and C. Dekker. Nano-optical tweezing of single proteins in plasmonic nanopores. *Small Methods, vol. 3, Issue 5*, 2019.

[21] C. Vuik, F.J. Vermolen, M.B. van Gijzen, and M.J. Vuik. *Numerical Methods for Ordinary Differential Equations*. Delft Academic Press, 2018.

[22] R. Yount, D. Babcock, W. Ballantyne, and D. Ojala. Adenylyl imidiodiphosphate, an adenosine triphosphate analog containing a p-n-p linkage. *ACS Publications*, 1971.

Appendices

.1 Calculating Realistic Values for Heat Flow Model

Parameters [7]:

$$\begin{aligned}
\lambda_g &= 318W/(mK) \\
\rho_g &= 19 \cdot 10^3 kg/m^3 \\
c_{v,g} &= 129J/(kgK) \\
c &= 1 \cdot 10^{12}/m^2 \\
h &= 10 \cdot 10^{-9} m \\
\rho_w &= 1 \cdot 10^3 kg/m^3 \\
\eta_w &= 8.9 \cdot 10^{-4} kg/(ms) \\
\beta_w &= 207 \cdot 10^{-6}/K \\
c_{p,w} &= 4.19 \cdot 10^3 J/(kgK) \\
g &= 9.81 m/s^2 \\
k_w &= \frac{\lambda_w}{\rho_w c_{p,w}} = 1.43 \cdot 10^{-7} m^2/s
\end{aligned} \tag{28}$$

We will need the dimensionless Rayleigh Number [18]:

$$Ra_L = \frac{\rho_w^2 \beta_w \Delta T L^3 g c_{p,w}}{\eta_w k_w} \approx 10^6 \tag{29}$$

Because for a horizontal hot plate in a flowing medium, with $Q = SA\Delta T$ (A is surface area), we have, when $10^5 < Ra_L < 2 \cdot 10^7$ [7]:

$$S = S_{up} + S_{down} = \frac{\lambda_g 0.54 Ra_L^{1/4}}{L} + \frac{\lambda_g 0.27 Ra_L^{1/4}}{L} = \frac{\lambda_g 0.81 Ra_L^{1/4}}{L} \approx 1.4 \cdot 10^9 W/(m^2 K) \tag{30}$$

.2 Setup Details

Here, we will show the setup as it is shown in the Experimental Methods section.

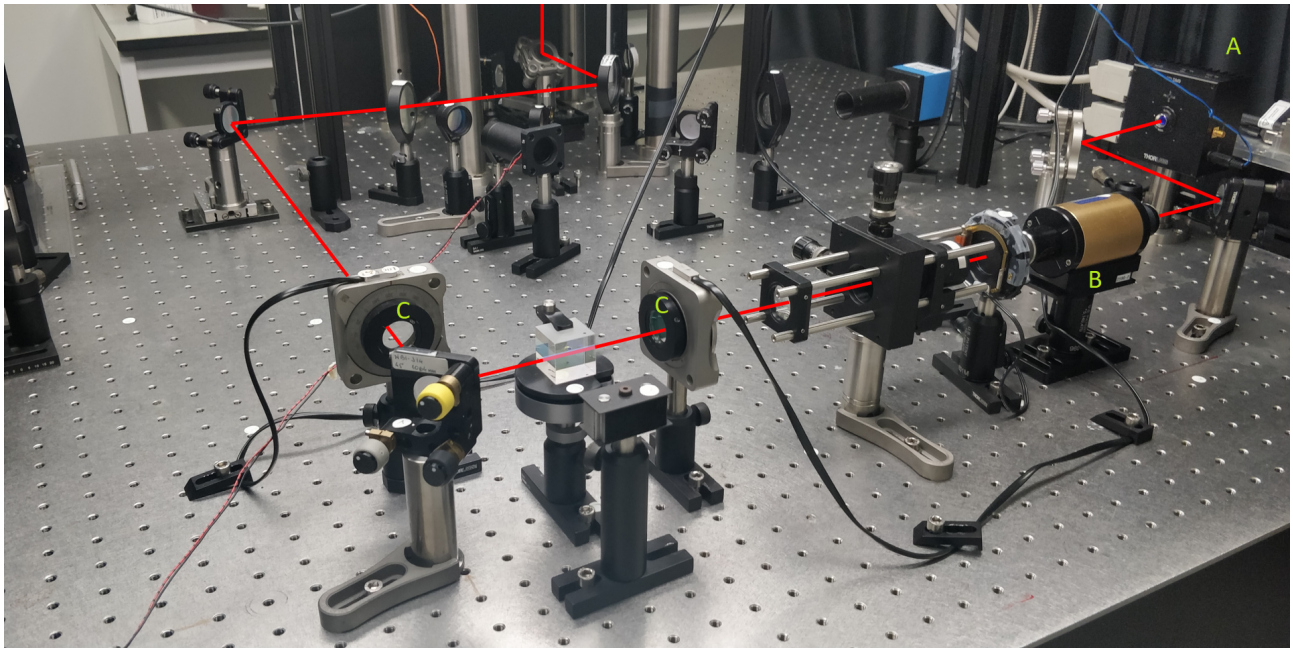

Figure 33: Photo taken of the setup. The laser is in the infrared part of the spectrum, and it has been visualised using a red line in this picture. Some components have been highlighted: A) is the laser and B) is the optical isolator used to prevent back reflection of the laser to the laser source. C) marks the two half-wave plates used for rotating the polarisation of the laser beam.

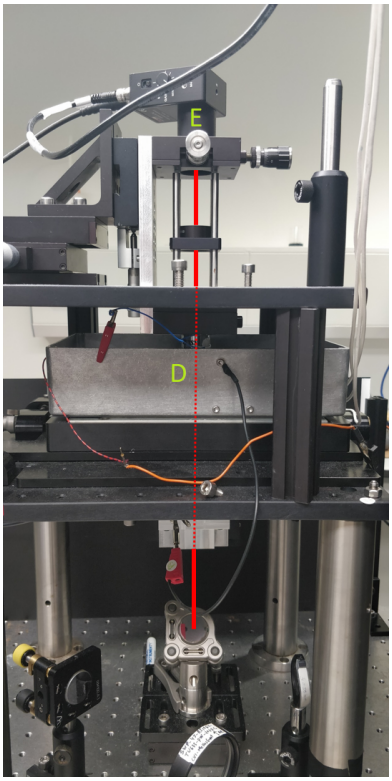

Figure 34: Photo of the next part of the setup. The laser beam has again been visualised in red. The laser travels upward through D), where the magnifying lenses are located and where the sample is mounted during the experiments. E) is the APD which records the signal.

.3 Other Traces

The longest HSP90 trap that we have recorded, was the following:

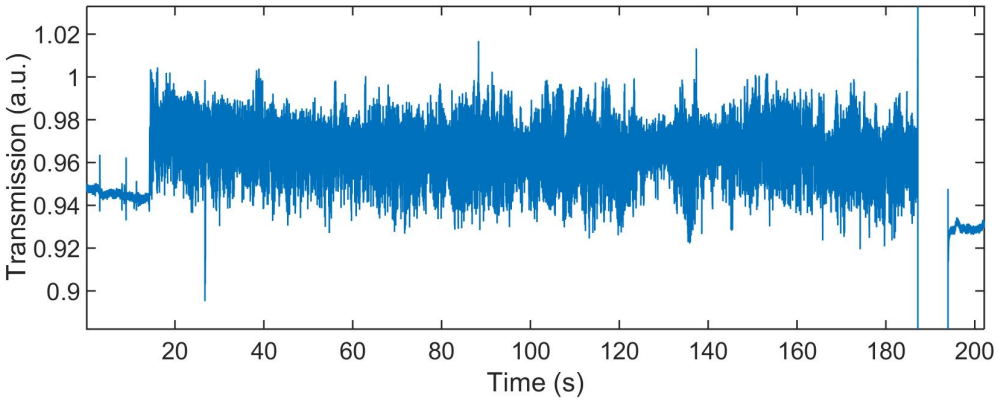

Figure 35: Longest recorded HSP90 trap, which lasts 3 minutes.

We also encountered cases where the particle got stuck in the aperture and would not leave after turning off the laser. It is therefore not possible to prove that the particle was trapped optically in these cases. An example is shown in figure 36.

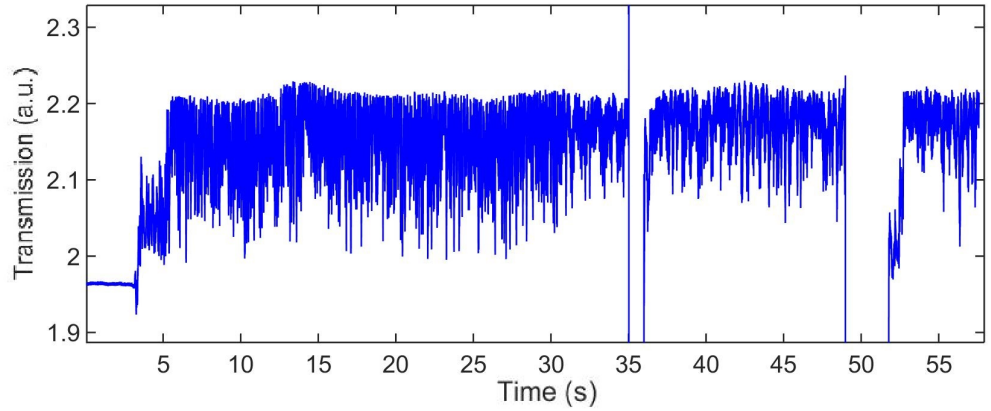

Figure 36: Trap where HSP90 with AMP-PNP gets stuck in the aperture. We see that is does not leave after turning off the laser.

Finally, we have also seen traces with drifting signal, shown in figure 37.

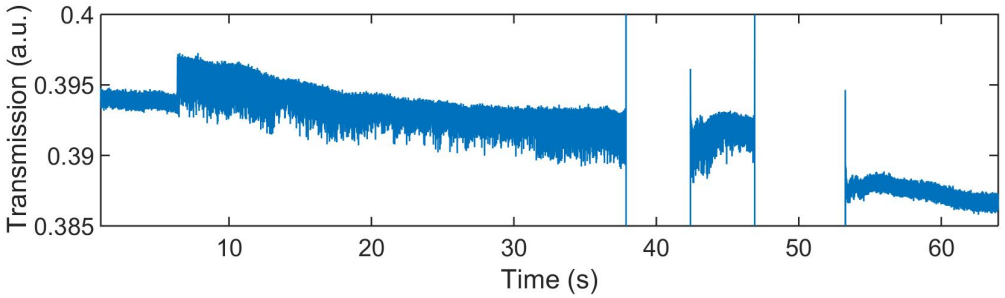

Figure 37: Bead trapping trace with drifting signal. We see that this trace clearly shows a drift, but not only linear drift. We need a more sophisticated method to correct for this than a linear correction.

.4 MATLAB code

Euler Forward for Heat Flow Model

```
R = 1e-5;
dr = 5e-8;
N = ceil(R/dr);
dt = 4.3e-15;
t_max = 2.5e-13;
i_max = t_max / dt;
r = (1:N)./N.*R;
S = 1.4e9;
Q = 20*2.5e10*exp(-4e12*r.^2).';
k = 1.3e-4;
u = zeros(N,1);
z = 1e-8;
lambda = 318;

H = zeros(N,1);
D2 = zeros(N);
D1 = zeros(N);

for i = 1:N
    for j = 1:N
        if i==j
            D2(i,j) = -2;
            D1(i,j) = -1;
        elseif i == j+1
            D2(i,j) = 1;
        elseif i == j-1
            D2(i,j) = 1;
            D1(i,j) = 1;
        end
    end
end
D2(1,2) = 2;
D2(N, N-1) = 2;
D2 = D2./(dr^2);
D1(N,N) = 0;
D1(N,N-1) = 0;
D1(1,2) = 0;
D1 = D1./(dr*ones(N,1)*r);
%D1 = zeros(N);


for i = 0:i_max
    du = k*D2*u+k*D1*u-S/z/lambda.*u+Q/z/lambda;
    u = u + dt*du;
    u(N) = 0;
end

U = u.';
plot(r,U);
```

3D Random Walk model

```
clear;
close all;
w = 50; %width
h = 30; %height
g = 10; %gap
d = 20; %depth
m = 100;
k = 0.2; %trap strength
b = 2; %damping constant
dt = 0.1;
a_avg = 0.02/sqrt(dt);
x = [0;0;0];
v = [0;0;0];
N = 3e3/dt;
count = zeros(w+2,h+2);
for i = 1:N
    phi = (asin(2*rand()-1)+pi/2);
    theta = 2*pi*rand();
    F = Force3(x(:,i), k, v(:,i), b);
    new_v = (a_avg * [sin(phi)*cos(theta); sin(phi)*sin(theta); cos(phi)] ...
    + F / m) + v(:,i);
    new_x = x(:,i) + dt * new_v;
    if inRange_v3(new_x, w,h,g,d) == 3
        new_v = -new_v;
    elseif inRange_v3(new_x, w,h,g,d) == 1
        a = sign(new_x(1)*new_x(2))*(h-g)/w;
        proj_a = (new_v(1)+a*new_v(2))/(1+a^2)*[1; a; 0];
        new_v = 2*proj_a - new_v + 2*[0; 0; new_v(3)];
    elseif inRange_v3(new_x, w,h,g,d) == 2 && sign(new_v(1)*new_x(1))==1
        new_v = [-new_v(1); new_v(2); new_v(3)];
    elseif inRange_v3(new_x, w,h,g,d) == 4
        disp('Particle escaped trap');
        break;
    end
    new_x = x(:,i) + dt * new_v;
    x = [x new_x];
    v = [v new_v];
    x_bar = round(new_x(1))+w/2+1;
    y_bar = round(new_x(2))+h/2+1;
    count(x_bar,y_bar)=count(x_bar,y_bar)+1;
end

scatter3(x(1,:),x(2,:),x(3,:),'.');
hold on;
plot([-w 0 w w 0 -w -w]/2,[h g h -h -g -h h]/2);
axis equal;
figure;
surf(count);
hold on;
plot([h g h -h -g -h h]/2+h/2+1.5,[-w 0 w w 0 -w -w]/2+w/2+1.5,'r');
```

```
function [ res ] = inRange_v3( theX, w, h, g, d )
% 0: in range
% 1: y out of range
% 2: x out of range
% 3: both out of range
% 4: z out of range
a = (h - g) / w;
b = g / 2;
res = abs(theX(2)) > b + a * abs(theX(1));
if abs(theX(1)) > w/2
    res = res + 2;
end
if abs(theX(3))>d/2
    res = 4;
end
end
```

```
function [ F ] = Force3( theX, k, theV, b )
if theX(1)~=0 && theX(2)~=0 && theX(3)~=0
    F = (-k*theX*(theX(1)^2+theX(2)^2+theX(3)^2) -b*theV);
else
    F = [0,0,0].';
end
end
```

Model for Generating Telegraph Noise

```
p1 = 2e-3;
p2 = 1e-3;
N = 1e5;
u = 0;
v = 0;
w = 0;
t = 0;
omega = 2 * pi * 1e3;
y = [];
y2= [];
for i = 1:N
    r = rand();
    if u==0 && r < p1
        u = 1 - u;
    elseif u==1 && r < p2
        u = 1 - u;
    end
    y = [y u];
end
plot(y);
hold on;
figure;
y_f = fft(y);
y_f = 2*(y_f(1:ceil(length(y_f)/2)));
y_f2 = fft(y2);
y_f2 = 2*(y_f2(1:ceil(length(y_f2)/2)));
loglog(abs(y_f(2:length(y_f))).^2);
```